

2

AD-A220 022

ELECTRON BEAM PUMPED XeF(C→A) LASER SCALING

Contract No. N00014-88-C-0418

Final Report for Period 1 July 1988 - 31 December 1989  
February 1990

Leonard N. Litzenberger and Alexander E. Mandl  
(617) 381-4564

DTIC  
ELECTE  
APR 4 1990  
S D

prepared for

OFFICE OF NAVAL RESEARCH  
800 N. Quincy Street  
Arlington, VA 22217-5000

prepared by

AVCO RESEARCH LABORATORY, INC.  
a subsidiary of TEXTRON, INC.  
2385 Revere Beach Parkway  
Everett, MA 02149

DISTRIBUTION STATEMENT A  
Approved for public release  
Distribution Unlimited

90 04 03 078

## REPORT DOCUMENTATION PAGE

1a. REPORT SECURITY CLASSIFICATION Unclassified			1b. RESTRICTIVE MARKINGS		
2a. SECURITY CLASSIFICATION AUTHORITY			3. DISTRIBUTION/AVAILABILITY OF REPORT		
2b. DECLASSIFICATION/DOWNGRADING SCHEDULE					
4. PERFORMING ORGANIZATION REPORT NUMBER(S)			5. MONITORING ORGANIZATION REPORT NUMBER(S)		
6a. NAME OF PERFORMING ORGANIZATION Avco Research Laboratory, Inc.		6b. OFFICE SYMBOL (If applicable)	7a. NAME OF MONITORING ORGANIZATION Office of Naval Research Dept. of Navy		
6c. ADDRESS (City, State and ZIP Code) Everett, MA 02149			7b. ADDRESS (City, State and ZIP Code) Arlington, VA 22217-5000		
8a. NAME OF FUNDING/SPONSORING ORGANIZATION Strategic Defense Initiative Org.		8b. OFFICE SYMBOL (If applicable)	9. PROCUREMENT INSTRUMENT IDENTIFICATION NUMBER N00014-88-C-0418		
8c. ADDRESS (City, State and ZIP Code) The Pentagon Washington, DC 20301-7100			10. SOURCE OF FUNDING NOS.		
			PROGRAM ELEMENT NO	PROJECT NO	TASK NO
			WORK UNIT NO		
11. TITLE (Include Security Classification) Electron Beam Pumped XeF(C+A) Laser Scaling					
12. PERSONAL AUTHOR(S) Litzenberger, Leonard N. and Mandl, Alexander E.					
13a. TYPE OF REPORT Final Technical		13b. TIME COVERED 88/07/01-89/12/31	14. DATE OF REPORT (Yr., Mo., Day) 1990 February		15. PAGE COUNT 65
16. SUPPLEMENTARY NOTATION					
17. COSATI CODES			18. SUBJECT TERMS (Continue on reverse if necessary and identify by block number)		
FIELD	GROUP	SUB GR	Xenon Fluoride, XeF, XeF(C+A), Rare Gas Halide Lasers, Excimer Lasers, Visible		
19. ABSTRACT (Continue on reverse if necessary and identify by block number) Efficient operation of the electron beam pumped XeF(C+A) laser under conditions which are scalable to large devices has been demonstrated. A five-component laser gas mixture at a pressure of 2.6 ATM was pumped at a rate of 290 kW/cm <sup>3</sup> with a 600-ns electron beam pulse. The laser gas mixture and output coupler reflectivity were carefully optimized under free-running conditions, and radiation was then injected into the stable cavity from an external flashlamp-pumped dye laser to reduce the flux buildup time to saturation levels. An intrinsic efficiency of 1.8% and a specific output energy of 3 J/l were demonstrated, and a total energy of 4 J was extracted from the e-beam excited medium. This scalable performance is superior to the performance previously achieved at a					
20. DISTRIBUTION/AVAILABILITY OF ABSTRACT UNCLASSIFIED/UNLIMITED <input type="checkbox"/> SAME AS RPT <input checked="" type="checkbox"/> DTIC USERS <input type="checkbox"/>			21. ABSTRACT SECURITY CLASSIFICATION Unclassified		
22a. NAME OF RESPONSIBLE INDIVIDUAL			22b. TELEPHONE NUMBER (Include Area Code)	22c. OFFICE SYMBOL	

high excitation rate ( $\sim 12 \text{ MW/cm}^3$ ), with a short e-beam pulse ( $\sim 10 \text{ ns}$ ) and at high gas pressure ( $\sim 6.5 \text{ ATM}$ ), by Rice University and United Technologies Research Center.

Through injection control the laser bandwidth was reduced, without a loss in efficiency, by more than two orders of magnitude, to less than  $1.3 \text{ \AA}$ , the resolution of the spectrometer. The laser wavelength was tuned from  $478.6 \text{ nm}$ , the lower limit of the dye that was used in the injection source, to  $486.8 \text{ nm}$ . The laser output energy varied by less than a factor of two when the injection source was tuned from a peak in the free-running laser spectrum to a valley, proving that continuous tuning is possible. Significantly narrower linewidths and a wider tuning range should be possible.

The small-signal net gain was measured during the excitation pulse at various wavelengths across the gain profile, and a peak gain of  $0.4\%/cm$  was recorded. The sidelight fluorescence spectrum was also recorded.

Because the  $\text{XeF(C}\rightarrow\text{A)}$  laser is continuously tunable over a large portion of the visible spectrum (from  $435$  to  $535 \text{ nm}$  or beyond) and can be operated either broadband or narrowband with high efficiency, it is potentially useful for a variety of applications, including submarine communication and detection, and target illumination and imaging. The successful operation of the  $\text{XeF(C}\rightarrow\text{A)}$  laser under conditions which are scalable to large systems represents a significant milestone in the development of laser technology needed to accomplish a variety of SDIO/ONR missions.

18. Lasers, Tunable Lasers, Narrowband Lasers, Electron Beam Pumped Lasers

# ACKNOWLEDGEMENT

The authors of this report gratefully acknowledge the technical assistance of A. Montagna, R. Fredholm and R. Tanguay during the experimental phase of this program, and helpful discussions with M. J. Smith and Dr. I. Itzkan who advised the authors on various aspects of optical resonator design and injection control.



STATEMENT "A" per Fred Quell  
ONR/Code 1220, Boston Office  
TELECON 4/3/90

VG

Accession For	
NTIS CRA&I	<input checked="" type="checkbox"/>
DTIC TAB	<input type="checkbox"/>
Unannounced	<input type="checkbox"/>
Justification	
By <i>per call</i>	
Distribution/	
Availability Codes	
Dist	Avail and/or Special
A-1	

## TABLE OF CONTENTS

<u>Section</u>	<u>Page</u>
List of Illustrations	v
List of Tables	vii
1.0 INTRODUCTION	1
2.0 DESCRIPTION OF DEVICE AND EXPERIMENTAL CONDITIONS	4
3.0 LASER OPTIMIZATION EXPERIMENTS	8
3.1 EXPERIMENTAL SETUP	8
3.2 GAS MIXTURE OPTIMIZATION	11
3.3 OUTPUT COUPLER REFLECTIVITY OPTIMIZATION	13
3.4 TEMPORAL CHARACTERISTICS	17
3.5 SPECTRAL CHARACTERISTICS	19
4.0 OTHER LASER GAS MIXTURES	28
5.0 MAXIMUM ENERGY EXTRACTION EXPERIMENT	32
6.0 SMALL-SIGNAL NET GAIN MEASUREMENTS	36
7.0 INJECTION-CONTROLLED OSCILLATOR EXPERIMENTS	40
7.1 EXPERIMENTAL SETUP	40
7.2 TEMPORAL CHARACTERISTICS	42
7.3 SPECTRAL CHARACTERISTICS AND WAVELENGTH TUNABILITY	47
7.4 SUMMARY OF INJECTION-CONTROLLED OSCILLATOR RESULTS	47
8.0 XeF(B $\rightarrow$ X) LASER PUMP FOR DYE LASER INJECTION SOURCE	51
9.0 COMPARISON WITH XeF(C $\rightarrow$ A) LASER PERFORMANCE AT HIGH E-BEAM PUMP RATE	54
10.0 CONCLUSIONS	56
References	57

# LIST OF ILLUSTRATIONS

<u>Figure</u>		<u>Page</u>
1	Photograph of e-beam pumped device	5
2	Schematic diagram of free-running oscillator experimental arrangement	9
3	E-beam energy deposition profiles in orthogonal directions	10
4	Sensitivity of the laser intrinsic efficiency to partial pressures of gases under free-running conditions	12
5	Sensitivity of laser intrinsic efficiency to output coupler reflectivity under free-running conditions	15
6	Sensitivity of laser intrinsic efficiency to intracavity flux under free-running conditions	16
7	Temporal pulse shapes for free-running oscillator (left side) and without laser oscillation (right side)	18
8	Temporal characteristics for varying output coupler reflectivity under free-running conditions	20
9	Temporal characteristics for varying $\text{NF}_3$ partial pressure under free-running conditions	21
10	Spectrum of unsuppressed sidelight fluorescence and of free-running laser output	22
11	Free-running laser spectrum at instrumental resolution of 0.13 nm (1.3 Å)	23
12	Unsuppressed sidelight fluorescence spectra for neon buffer and varying krypton partial pressure	25
13	Unsuppressed sidelight fluorescence spectra for argon buffer and varying krypton partial pressure	26
14	Unsuppressed sidelight fluorescence spectra with and without xenon and krypton	27
15	Temporal characteristics for neon buffer and varying krypton partial pressure, under free-running conditions	30
16	Schematic diagram of experimental setup for maximum energy extraction	33
17	Temporal pulse shapes for free-running oscillator with 3-in. diameter mirrors (left side) and without laser oscillation (right side)	34

<u>Figure</u>		<u>Page</u>
18	Temporal waveforms during small-signal net gain measurement at 476.5 nm	37
19	Small-signal net gain as a function of time during e-beam pulse, at varying wavelength	38
20	Small-signal net gain as a function of wavelength	39
21	Schematic diagram of setup for injection-controlled oscillator experiments	41
22	Temporal pulse shapes for free-running oscillator (left side) and injection-controlled oscillator (right side)	43
23	Predicted laser turn-on time as a function of output coupler reflectivity for varying flux incident upon the output coupler	45
24	Laser signal amplitude as a function of time for injection-controlled and free-running oscillators	46
25	Comparison of free-running oscillator laser spectrum (left side) with injection-controlled oscillator spectra at varying injected wavelength (right side)	48
26	Temporal pulse shape of injection-controlled laser output at varying injected wavelength	49
27	Optimization of XeF(B→X) lasing with XeF(C→A) laser gas mixture	52
28	Temporal characteristics for XeF(C→A) laser gas mixture and XeF(B→X) mirrors	53

## LIST OF TABLES

<u>Table</u>		<u>Page</u>
1	Experimental Conditions	6
2	Optimized Laser Gas Mixture	14
3	XeF(B)→XeF(C) Transfer Rate Constant $k_{BC}$	29
4	Summary of Free-Running Oscillator Results	35
5	Summary of Results with Injection	50
6	Demonstrated XeF(C→A) Laser Performance at Low and High E-Beam Pump Rates	55

## 1.0 INTRODUCTION

Among the gas lasers, the XeF(C $\rightarrow$ A) laser is of special interest because it is continuously tunable over a large portion of the visible spectrum (from 435 to 535 nm or beyond), and it can be operated either broadband or narrowband with high efficiency. Hence, it is potentially useful for such applications as submarine communication and detection, and target illumination and imaging.

Most of the research performed to date on this laser system, using direct electron beam (e-beam) pumping, has been done by researchers at Rice University and United Technologies Research Center (UTRC), at a very high excitation rate ( $\sim 12 \text{ MW/cm}^3$ ), with a short e-beam pulse ( $\sim 10 \text{ ns}$ ) and at high gas pressure ( $\sim 6.5 \text{ ATM}$ ). The most recent results obtained under these conditions have been published in Ref. 1.

The attainment of such a high excitation rate requires the generation of an electron beam with a very high current density ( $250 \text{ A/cm}^2$  or higher, dependent upon the gas density). At this current density level and short e-beam pulse duration, stray inductance within the pulsed power supply severely limits the size and energy to which the e-beam and, hence, the laser can be scaled. The high gas pressure also places severe constraints on the design of the foil window support and the laser cavity windows. The highest output energy obtained under these operating conditions is  $0.7 \text{ J}$ .<sup>1</sup>

Successful scaling of the XeF(C $\rightarrow$ A) laser to high energies requires a substantial reduction in the e-beam current density and excitation rate, and a significant increase in the duration of the e-beam pulse. With this in mind, Avco Research Laboratory undertook an investigation of XeF(C $\rightarrow$ A) lasing at a much lower e-beam pump rate of  $250 \text{ kW/cm}^3$  and a gas pressure of  $1.6 \text{ ATM}$ , as part of the Laboratory's 1987 IRAD program. This investigation showed that the XeF(C $\rightarrow$ A) laser does operate efficiently at low excitation rate.<sup>2</sup> In contrast to the afterglow lasing observed without injection at high excitation rate,<sup>3</sup> lasing was observed during the 700-ns excitation pulse.

Nighan et al<sup>4</sup> had previously argued that high pump rates are required for efficient laser energy extraction, to ensure that the intracavity flux builds up to saturation levels before the e-beam pulse is terminated and the C state is collisionally deactivated. This argument is only valid for e-beam

pulses of fixed short duration ( $\sim 10$  ns). When the e-beam pulse is extended to many times the C-state lifetime ( $\sim 40$  ns), the population inversion reaches steady state early in the e-beam pulse, longer flux buildup times become acceptable, and the medium can be pumped at a greatly reduced rate.

The intrinsic efficiency of 0.7% that was obtained during these first successful experiments at low pump rate represented a lower bound to what was attainable, due to the fact that the laser gas mixture and resonator output coupler reflectivity had not been optimized for the low pump rate conditions. In addition, it was clear that significantly higher efficiencies could be achieved by injecting radiation into the cavity from an external source, so as to reduce the flux buildup time to saturation levels. Without injection, lasing occurred during the final 400 ns of the 700-ns excitation pulse.

Accordingly, Avco Research Laboratory proposed that additional experiments be conducted under scalable, low pump rate conditions, to establish the ultimate laser efficiency and specific output energy. Avco also proposed that line-narrowing and wavelength tuning experiments be performed under the same conditions. These proposals to ONR led to the award of the current contract. This report presents the results of the experimental investigation which was conducted under this program.

In brief summary, the performance of the XeF(C $\rightarrow$ A) laser, pumped at a rate of  $290 \text{ kW/cm}^3$  with a 600-ns e-beam pulse, has been substantially improved by a careful optimization of the laser gas mixture and output coupler reflectivity, and by injecting radiation into the cavity from an external source. An intrinsic efficiency of 1.8% and a specific output energy of 3 J/l have been achieved, and a total energy of 4 J has been extracted from the excited medium. This performance which was obtained under scalable operating conditions is superior to that achieved by Rice University and UTRC at high excitation rate. (The corresponding values at  $12 \text{ MW/cm}^3$  and a 10-ns e-beam pulse duration are 1.2%, 1.5 J/l and  $0.7 \text{ J.l}^{-1}$ .) The laser pulse duration was 500 ns (FWHM).

Through injection control, the laser bandwidth has been reduced, without a loss in efficiency, by more than two orders of magnitude to less than  $1.3 \text{ \AA}$ , the resolution of the spectrometer. In addition, the laser wavelength has been tuned from 478.6 nm, the lower limit of the dye that was used in the injection source, to 486.8 nm. The XeF(C $\rightarrow$ A) laser output energy varied by less than a factor of two when the injection source was tuned from a peak in

the free-running laser spectrum to a valley, proving that continuous tuning is possible. Significantly narrower linewidths and a wider tuning range should be possible.

The small-signal net gain was also measured during the e-beam excitation pulse at various wavelengths across the gain profile, by passing a CW argon-ion laser beam through the excited medium. A peak gain of 0.4%/cm was recorded. The sidelight fluorescence spectrum was measured under various conditions.

Section 2.0 of this report describes the device on which the experiments were performed and the general operating conditions. The results of the gas mixture and output coupler reflectivity optimization studies, performed under free-running conditions, are presented in Sec. 3.0. The temporal and spectral characteristics of the free-running laser output are also described in this section. Section 4.0 discusses other gases which were tested as part of the laser gas mixture, in an effort to achieve further improvements in laser performance, and Sec. 5.0 describes an experiment in which a higher output energy was attained by installing larger diameter mirrors on the laser cavity. The measurements of the small-signal net gain are presented in Sec. 6.0. The improvements in laser performance achieved with injection are the subject of Sec. 7.0. The feasibility of extracting XeF(B $\rightarrow$ X) laser radiation from a portion of the e-beam excited medium, for the purpose of pumping a dye laser injection source, is discussed in Sec. 8.0. Section 9.0 compares the XeF(C $\rightarrow$ A) laser performance achieved in our experiments under scalable operating conditions with that obtained by Rice University and UTRC at high excitation rate, short e-beam pulse duration and high gas pressure. Concluding remarks are made in Sec. 10.0.

## 2.0 DESCRIPTION OF DEVICE AND EXPERIMENTAL CONDITIONS

A photograph of the device which was used in the experiments is presented in Fig. 1. The electron beam which excited the laser gas was produced by a cold-cathode (i.e., graphite felt) electron gun, or diode. The e-beam entered the pressurized laser cavity from the evacuated electron gun through a 75- $\mu$ m-thick Kapton foil window which was supported by an hibachi-like structure. [The foil was coated with a thin layer ( $\sim 200$  Å) of aluminum on the side which faced the electron gun.]

The e-beam dimensions were 10.8 cm x 103 cm at the cathode. The e-beam was spatially compressed by a factor of approximately 2.5 in the shorter direction in a convergent applied magnetic field within the "drift region" between the mesh anode and the foil window. This feature served to minimize plasma closure effects within the diode by reducing the magnetic field strength within the diode and by allowing the use of a larger anode-to-cathode spacing (7.4 cm) for the required current density in the gas. The magnetic field strength within the laser cavity was 2 kG. The magnetic field served to limit the amount of electron diffusion within the gas, caused by scattering within the foil window and within the laser gas.

The overall dimensions of the opening in the foil support structure through which the e-beam entered the gas were 4 cm x 100 cm. This defined two dimensions of the excited volume. The third dimension of 9.2 cm was defined by the distance from the foil window to the rear wall of the laser cavity.

The electron gun was powered by a three-stage Marx generator with bipolar charging. Each of the six 2- $\mu$ f Marx capacitors was charged to 67.5 kV before the system was fired. The erected Marx voltage pulse was terminated before significant droop had occurred, by firing a crowbar switch located at the Marx output. A 3-ohm electrolytic resistor placed in series with the Marx generator limited the rate of capacitor discharge during crowbar operation, to protect the Marx capacitors. During the e-beam pulse, approximately 20% of the erected Marx voltage was dropped across this resistor.

Table 1 lists the conditions under which the experiments were performed. The e-beam energy input was determined from the rise in gas pressure following the e-beam pulse caused by e-beam heating of the gas, and from the heat capacity of the gas at constant volume. The ideal gas law was

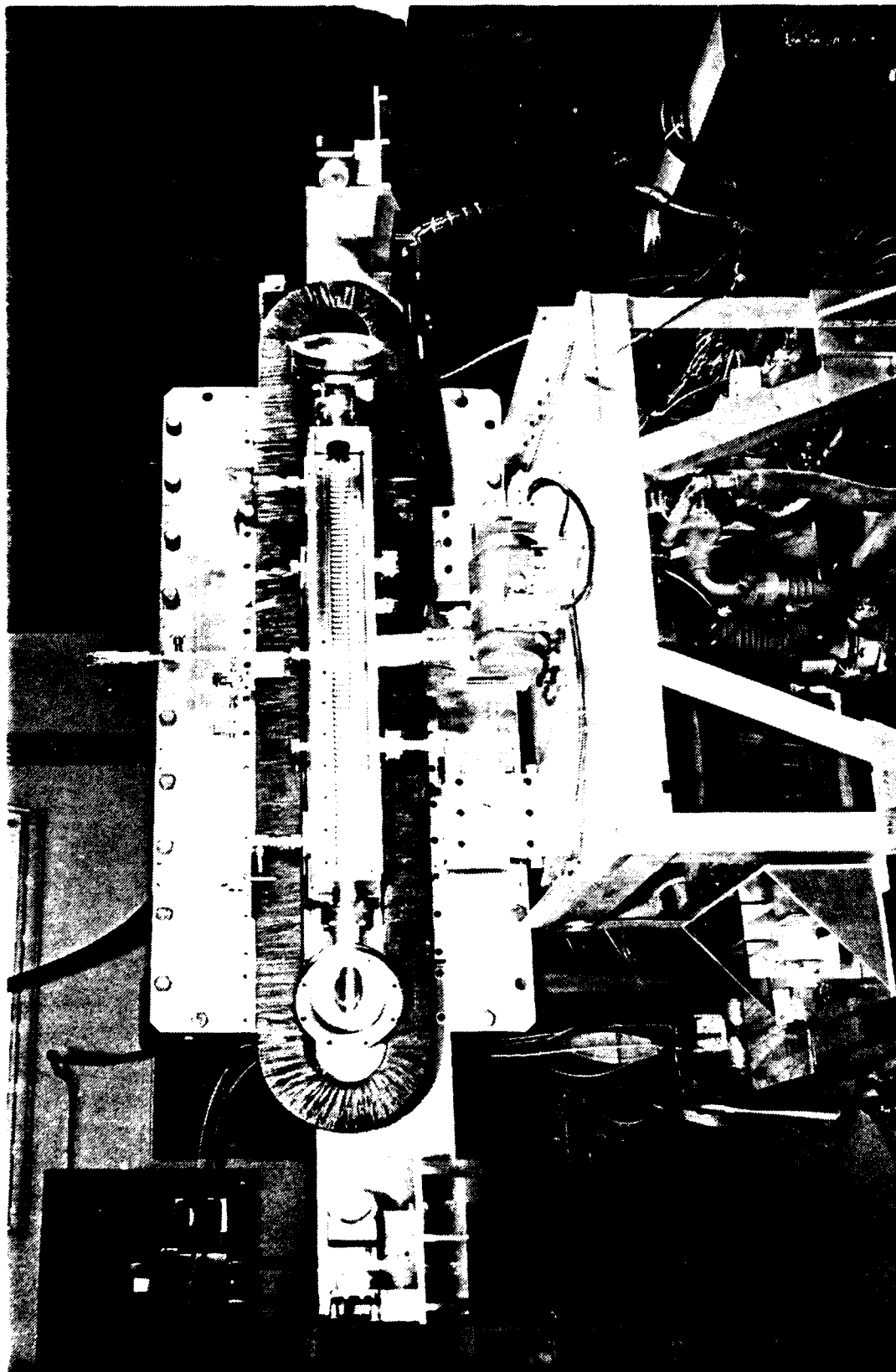


Figure 1. Photograph of e-beam pumped device. (Brewster-angle windows were replaced with normal-incidence mirrors/windows during the experiments.)

N6113

TABLE 1. EXPERIMENTAL CONDITIONS

E-beam pump rate	290 kW/cm <sup>3</sup>
E-beam pulse duration	600 ns
Specific energy input	170 J/liter
Gas temperature	300 °K
Gas pressure	2.6 ATM
Medium gain length	1 m
Optical resonator	Internal plano-concave

assumed, and the ratio of the excited volume to the total cavity volume was taken into account. A small correction was made for radiation losses. The energy input determined in this fashion was consistent, within the experimental uncertainties, with measurements of the e-beam voltage and current entering the gas, made with a resistive voltage divider, and with a current collection plate and pair of pulse current transformers, respectively.

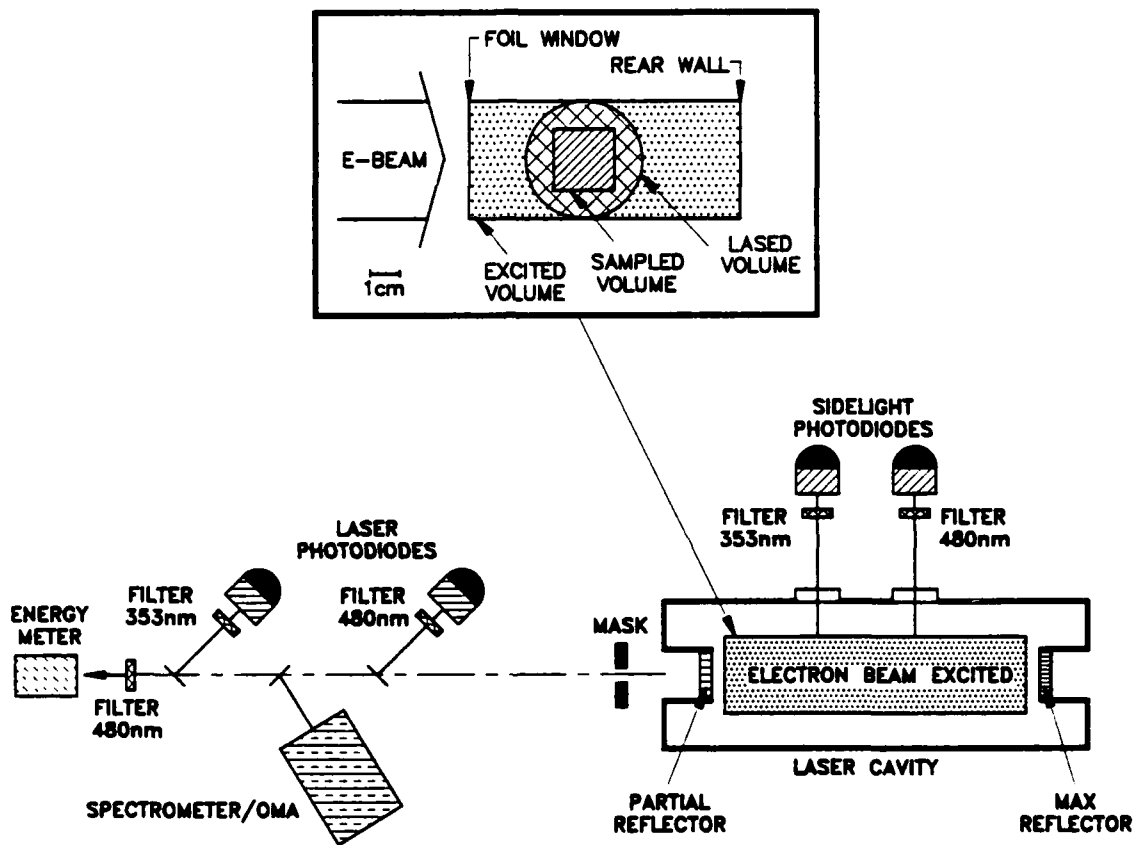
### 3.0 LASER OPTIMIZATION EXPERIMENTS

#### 3.1 EXPERIMENTAL SETUP

The laser gas mixture and output coupler reflectivity were optimized under free-running conditions, using the setup shown in Fig. 2. A stable, plano-concave cavity consisting of 2-in.-diameter mirrors was mounted on the device. The mirrors were mounted internally, 120 cm apart in a reentrant geometry, to minimize cavity losses and the flux buildup time. The mirrors served also as the pressure windows for the gas cell.

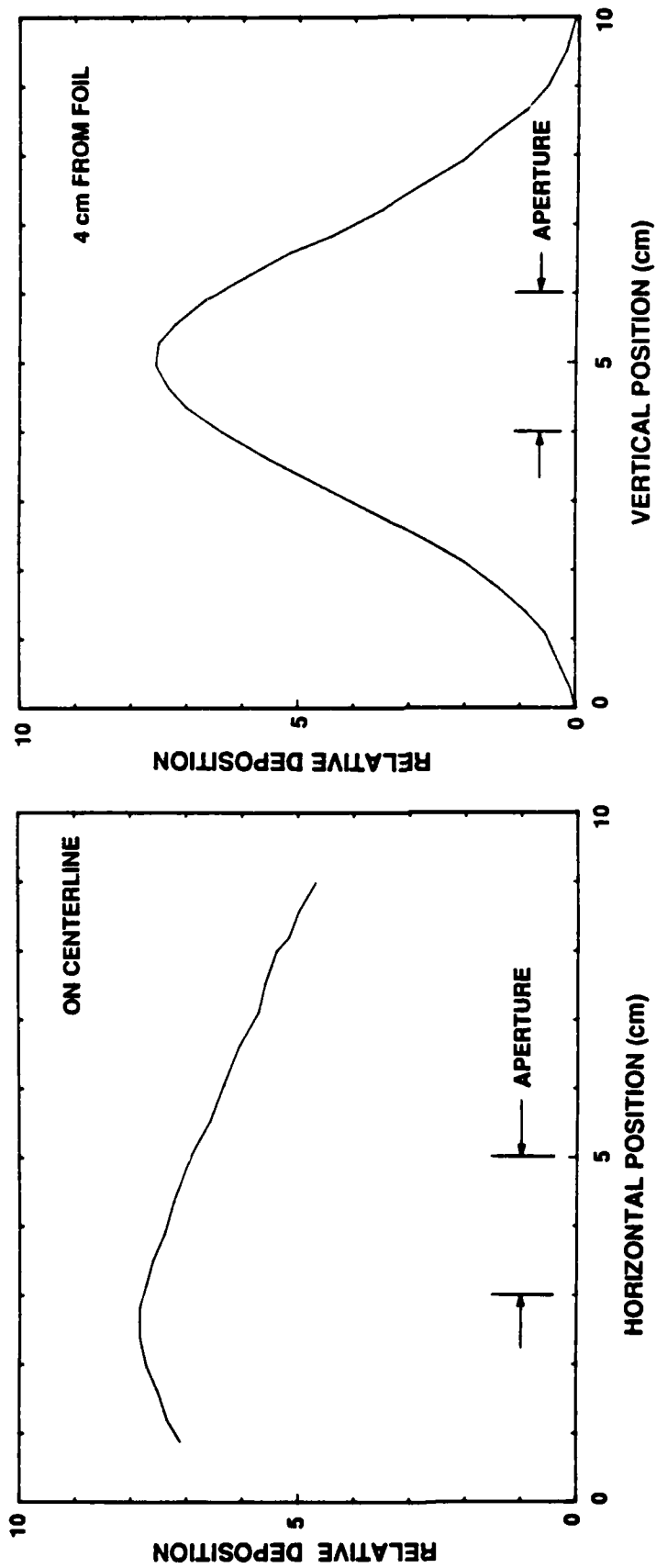
The maximum reflector (99.7% R) had a radius of curvature of 10 m, while the output coupler was flat. The mirrors were coated with a dielectric stack on the side which faced the laser gas so that the mirrors would reflect from 460 to 500 nm. The coatings were designed to have minimum reflectivity ( $R < 20\%$ ) at XeF(B $\rightarrow$ X) laser wavelengths (349-354 nm), in order to suppress XeF(B $\rightarrow$ X) laser oscillations which would have competed with collisional transfer of population from the B state to the C state. The outer mirror surface was anti-reflection (AR) coated from 350 to 500 nm.

The mirrors had a clear aperture of 3.8-cm diameter and were mounted 4 cm from the foil window through which the e-beam entered the gas. While lasing was allowed to occur over the entire clear area, a central 2 cm x 2 cm region was selected for diagnosis, using a mask placed just beyond the laser output. The purpose of this mask was to select a region which was uniformly pumped ( $\pm 10\%$ ) by the e-beam. The spatial distribution of the deposited e-beam energy was determined beforehand, using a technique described in Ref. 5. In that measurement fluorescence emitted by the excited gas was photographed through an end window of the cavity under non-lasing conditions. The intensity of XeF(B $\rightarrow$ X) fluorescence at  $\sim 350$  nm had previously been shown to be very nearly proportional to the amount of energy deposited by the e-beam.<sup>5</sup> Therefore, XeF(B $\rightarrow$ X) fluorescence was photographed, using a gas mixture which did not contain krypton but which had a stopping power identical to that of the XeF(C $\rightarrow$ A) laser gas mixture. The deposition profiles measured using this technique are displayed in Fig. 3. We verified that the shapes of the profiles were independent of the absolute e-beam current density entering the gas, and of the fluorescence intensity and film exposure level. The profiles were only dependent upon the voltage, gas pressure and gas



P1245

Figure 2. Schematic diagram of free-running oscillator experimental arrangement. The inset shows an end-on view of the laser cavity (to scale).



N8775

Figure 3. E-beam energy deposition profiles in orthogonal directions. The e-beam foil window was located at the origin of the horizontal axis.

composition. The pump rate and specific energy input values quoted in Table 1 refer to the 2 cm x 2 cm sampled region.

The laser output energy that passed through the aperture of the mask was measured with a 4-in.-diameter, surface-absorbing calorimeter (Scientech, Inc., model 36-0401/36-4002). The calorimeter was calibrated in situ by delivering a known amount of electrical energy to resistive heaters embedded within the meter. (The uncertainty in the calorimeter calibration was  $\pm 5\%$ .) A color glass filter which only transmitted at wavelengths longer than 385 nm (Schott GG385) was placed in front of the calorimeter to ensure that the calorimeter did not see any XeF(B $\rightarrow$ X) or KrF(B $\rightarrow$ X) radiation which might have been present. The energy meter readings were corrected for losses on the uncoated optics which were located between the meter and the laser cavity.

The temporal characteristics of the laser output and of the sidelight fluorescence were recorded with vacuum photodiodes (Hamamatsu Corp., model R1193U-02) which were outfitted with appropriate bandpass and edge filters. Neutral density filters were also employed to ensure a linear photodiode response. Both XeF(B $\rightarrow$ X) and XeF(C $\rightarrow$ A) emissions were recorded, although no XeF(B $\rightarrow$ X) laser radiation was detected in any of the experiments.

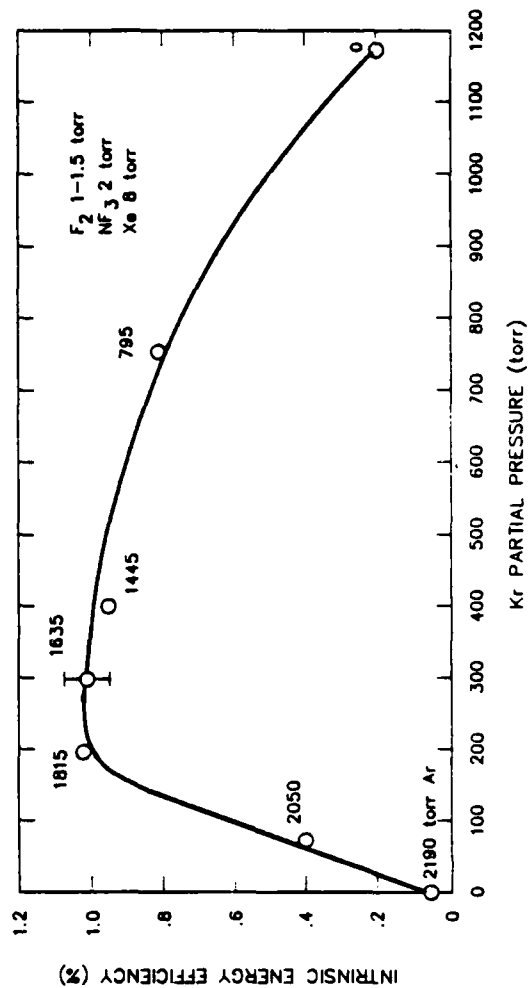
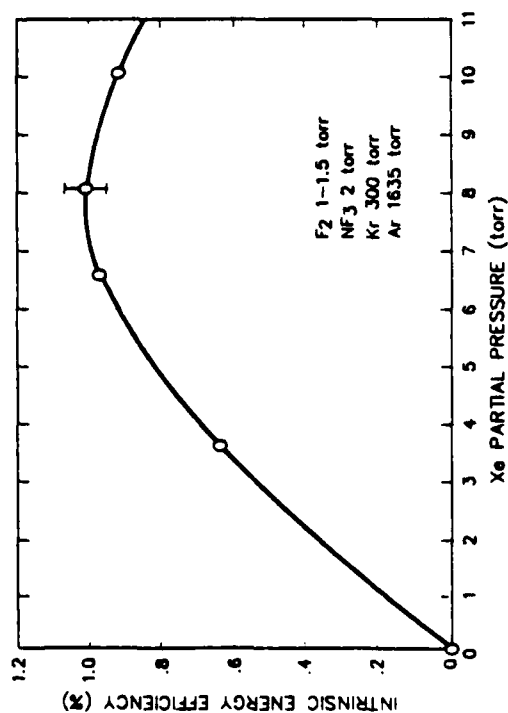
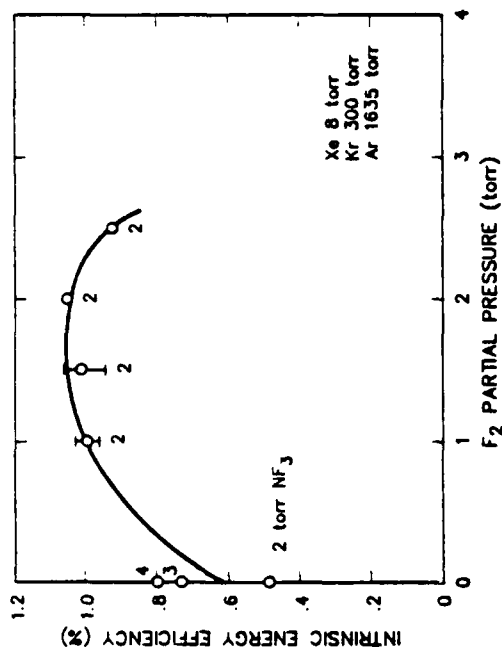
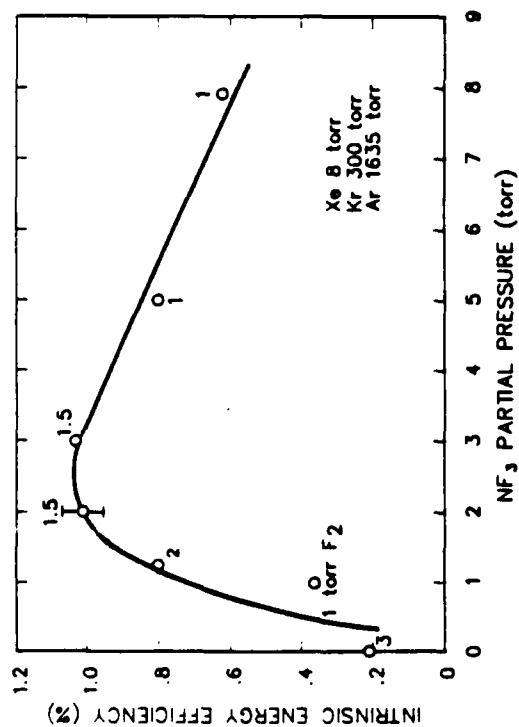
The temporally integrated laser spectrum was recorded with a 0.5-m grating spectrometer (Jarrell-Ash Co., model 82-536) which was coupled to an optical multichannel analyzer (EG&G Princeton Applied Research, model 1421/1460). Wavelength calibration of this instrument was performed using an argon-ion laser. The argon-ion laser was also used to measure the resolution of the spectrometer.

### 3.2 GAS MIXTURE OPTIMIZATION

The results of the gas mixture optimization experiments are presented in Fig. 4. High purity, research grade gases were premixed in a separate tank before introduction to the laser cavity. Good mixing was ensured by feeding the gases through a "piccolo" tube which ran down the center of the tank. The tank, the laser cavity and all associated plumbing were passivated beforehand by prolonged exposure to fluorine.

The laser cavity was constructed from nonmagnetic stainless steel, and the internal walls were plated with nickel. The cavity was evacuated with an

REFLECTIVITY 86.5%



N8768

Figure 4. Sensitivity of the laser intrinsic efficiency to partial pressures of gases under free-running conditions.

oil diffusion pump, equipped with a cryogenic trap, before it was filled with laser gas. The laser cavity was filled with fresh gas prior to each shot.

The partial pressure of each of the gas constituents was varied in order to determine the optimum gas mixture. As the partial pressure of a given halogen was varied, the partial pressure of the other halogen was simultaneously adjusted to maintain approximately the same total halogen pressure. In addition, as the partial pressure of krypton was changed, the partial pressure of argon was adjusted to maintain the same total e-beam stopping power and, hence, approximately the same e-beam pump rate.

The gas mixture which was found to be best and was, therefore, used in all subsequent experiments is listed in Table 2. As had previously been observed under high pump rate conditions,<sup>6</sup> eliminating any of the gas constituents resulted in poorer laser performance. The optimum mixture of gases was somewhat different, though, from that found to be best at high pump rate. A reduced partial pressure of  $\text{NF}_3$  gave the best results at low pump rate. Nitrogen trifluoride is an effective electron attacher at electron energies above 1 eV. A high partial pressure ( $\sim 8$  Torr) was required at high pump rate, probably to limit the electron density and minimize photoabsorption by excited rare-gas atomic species.

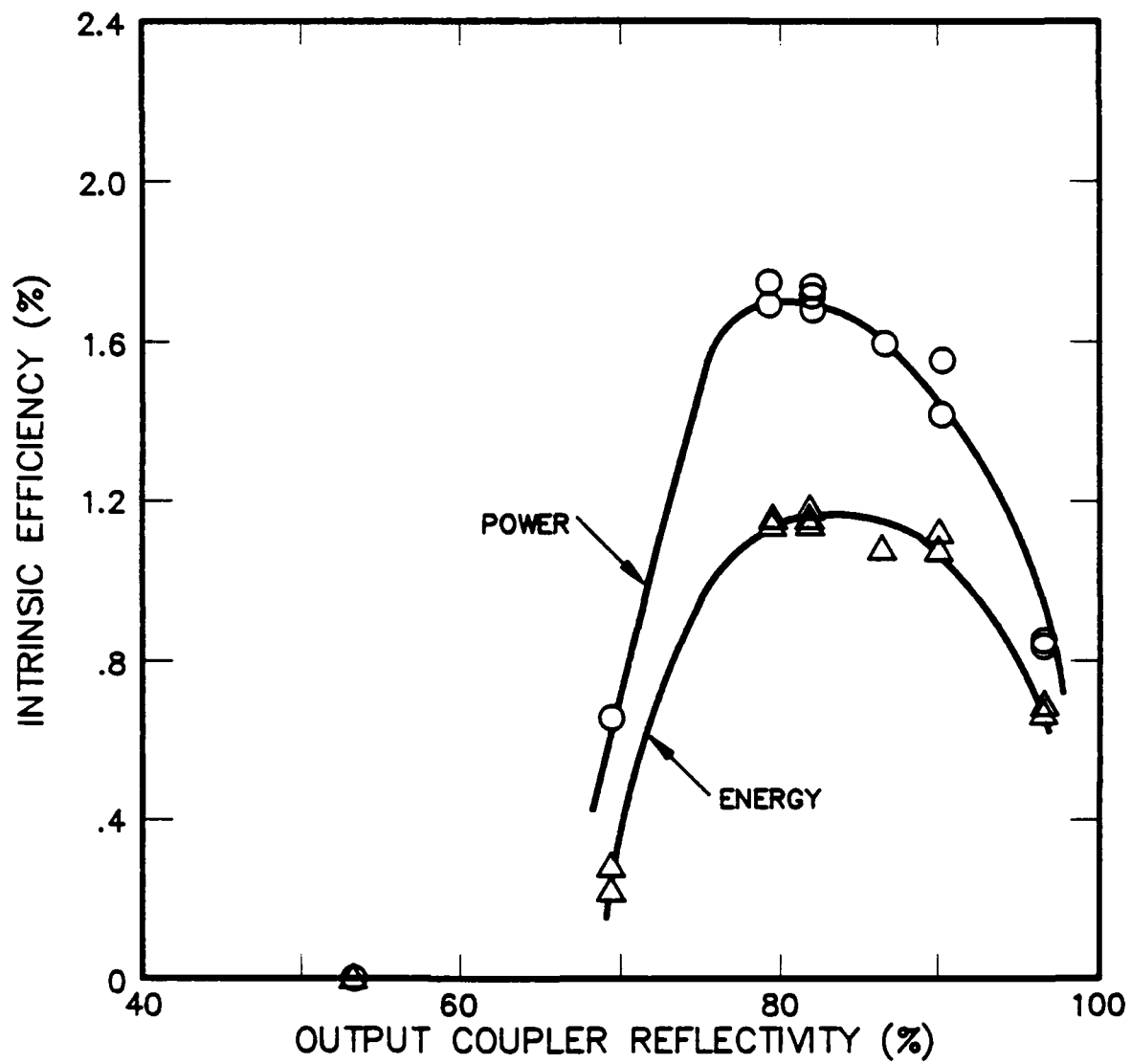
### 3.3 OUTPUT COUPLER REFLECTIVITY OPTIMIZATION

The reflectivity of the output coupler was then optimized, using the optimum laser gas mixture. The results are displayed in Fig. 5. Both energy and power efficiency values are given (uncertainty  $\pm 10\%$ ). The energy efficiency is the ratio of the laser output energy and the total amount of energy deposited within the sampled region during the e-beam pulse. The power efficiency, on the other hand, counts only the energy that was deposited following laser turn-on. The high power efficiency values in Fig. 5 provided an early indication of the substantial improvement in efficiency which would later be achieved by injection.

The same data are plotted in an alternate fashion in Fig. 6. The intracavity flux was determined from the output flux and the resonator output coupling. Intracavity flux levels in the range of  $4 \text{ MW/cm}^2$  were required to ensure efficient energy extraction. This is consistent with the calculated saturation intensity of  $\sim 1.5 \text{ MW/cm}^2$ .

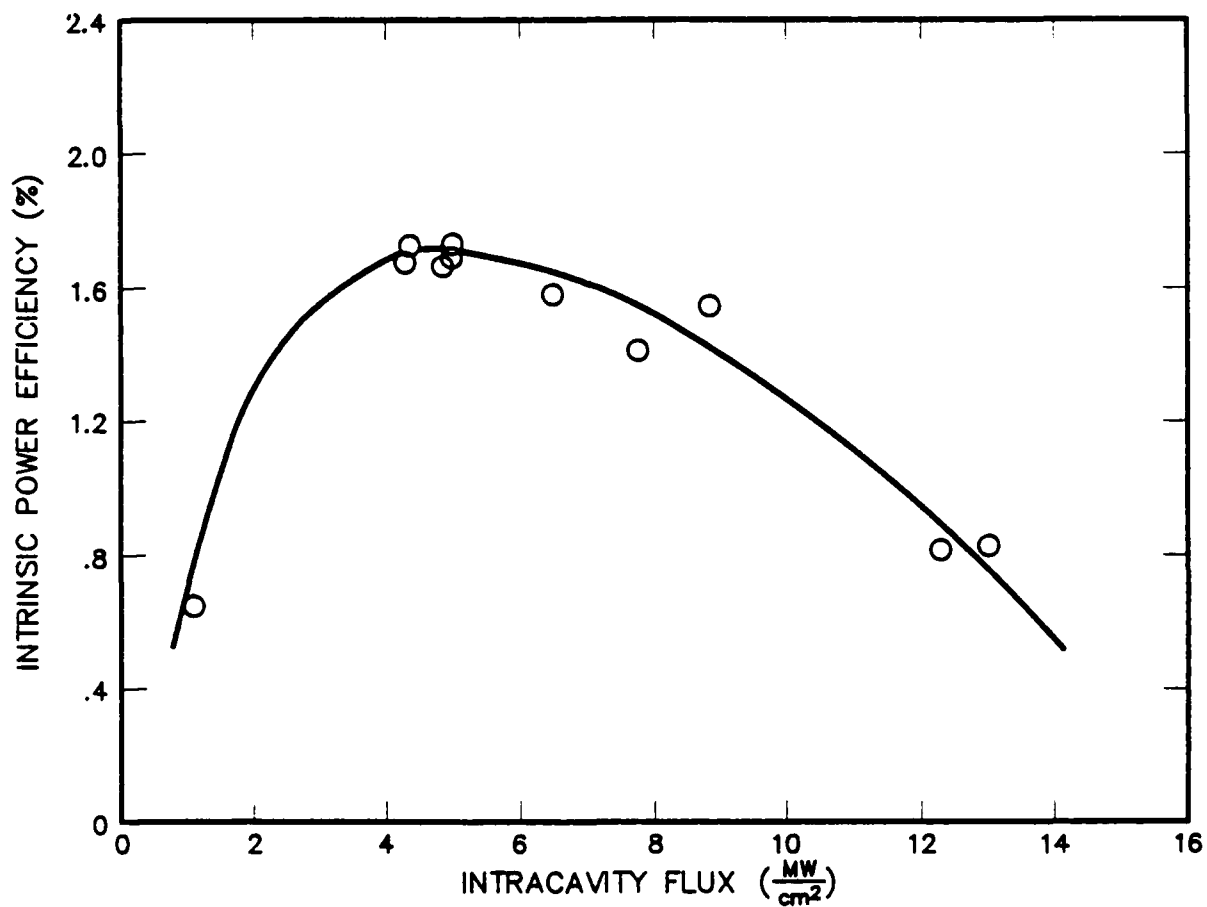
TABLE 2. OPTIMIZED LASER GAS MIXTURE

$F_2$	1.5 Torr
$NF_3$	2 Torr
Xe	8 Torr
Kr	300 Torr
Ar	1635 Torr



M9325 - 1

Figure 5. Sensitivity of laser intrinsic efficiency to output coupler reflectivity under free-running conditions.



M9324 -1

Figure 6. Sensitivity of laser intrinsic efficiency to intracavity flux under free-running conditions.

### 3.4 TEMPORAL CHARACTERISTICS

The temporal characteristics of the laser output and of the sidelight fluorescence under optimized, free-running conditions are shown in Fig. 7. Also shown are the e-beam voltage and current waveforms. The current waveforms were measured with a current collection plate mounted within the laser cavity and a pair of pulse current transformers. (This accounts for the duality of signals.) Because the voltage and current were both relatively constant in time during the 600-ns pulse, the pump rate was reasonably constant. The finite voltage and current risetimes were largely a consequence of stray inductance ( $\sim 1.3 \mu\text{H}$ ) within the Marx generator.

Sidelight temporal characteristics are shown, both with lasing (left side) and without lasing (right-hand side) in Fig. 7. Lasing and amplified spontaneous emission were temporarily prevented by misaligning the resonator mirrors and by physically blocking the two halves of the 1-m-long gain medium from one another.

The unsuppressed  $\text{XeF}(\text{C} \rightarrow \text{A})$  sidelight fluorescence signal exhibited a slow, steady decline during the pulse, while the  $\text{XeF}(\text{B} \rightarrow \text{X})$  sidelight signal displayed a more dramatic increase. These opposite trends probably reflected a redistribution of populations between the closely spaced B and C states (spacing  $\sim 700 \text{ cm}^{-1}$ ), caused by e-beam heating of the gas. The gas temperature rise was 130°K. In a separate experiment, the gas temperature rise was reduced to approximately 90°K by replacing a portion of the argon buffer, specifically 135 Torr, with 1000 Torr of helium. This served to increase the total gas density by nearly 50% while maintaining the same total e-beam stopping power and, hence, approximately the same specific energy input. However, this led to a 30% decline in laser output rather than the hoped-for increase.

The C-state lifetime (including quenching) was of the order of 40 ns. This long lifetime led to a persistence of the fluorescence following the termination of the e-beam pulse.

Both  $\text{XeF}(\text{C} \rightarrow \text{A})$  and  $\text{XeF}(\text{B} \rightarrow \text{X})$  sidelight fluorescent emissions were partially suppressed by lasing on the  $\text{XeF}(\text{C} \rightarrow \text{A})$  transition, reflecting the high degree of coupling between the B and C states. The C state is believed to be formed through the B state.

Lasing was observed during the e-beam excitation pulse rather than primarily in the afterglow, as was the case in the high pump rate experiments,

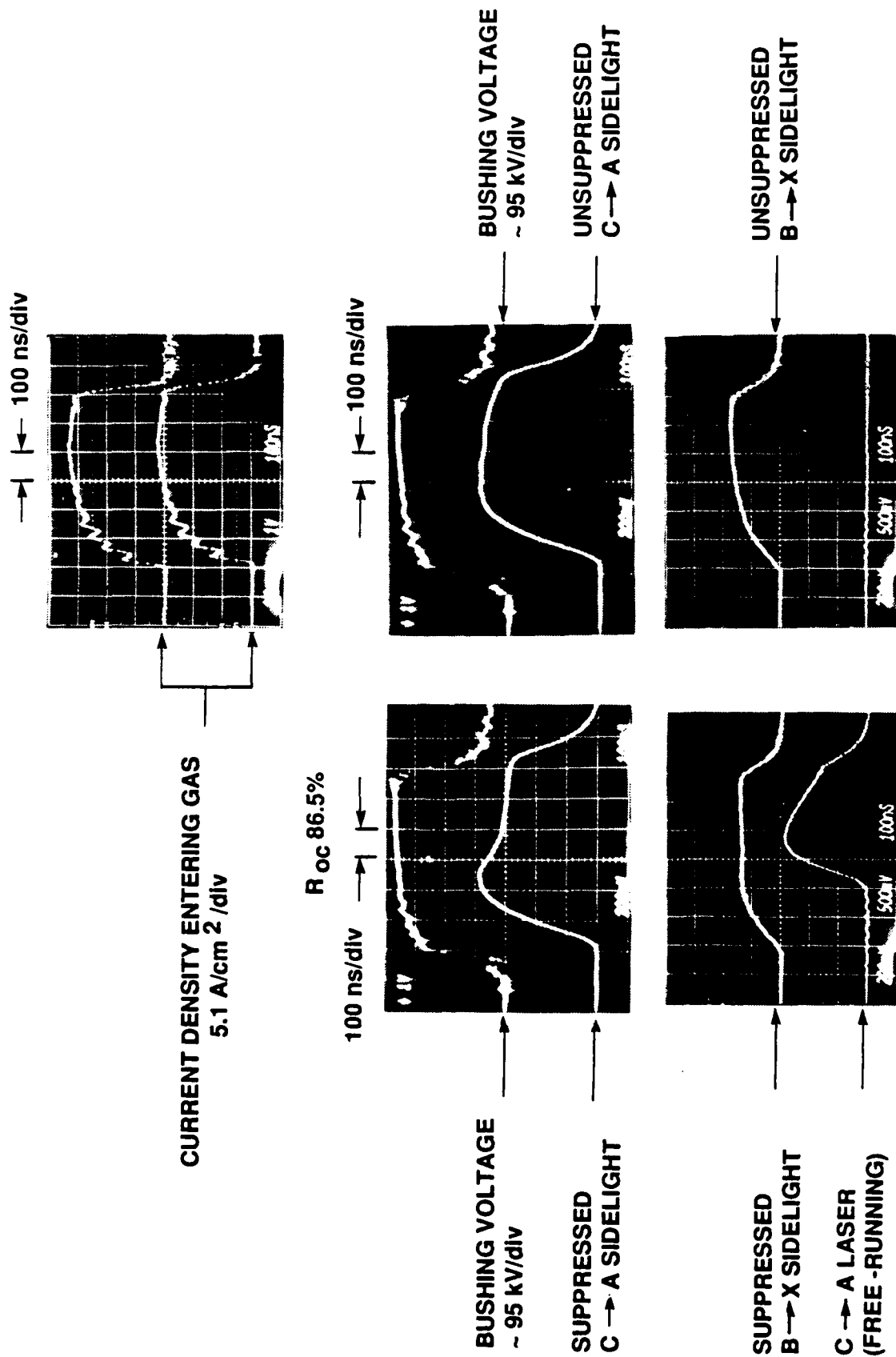


Figure 7. Temporal pulse shapes for free-running oscillator (left side) and without laser oscillation (right side). Current waveforms are also shown (upper right photograph).

N8762

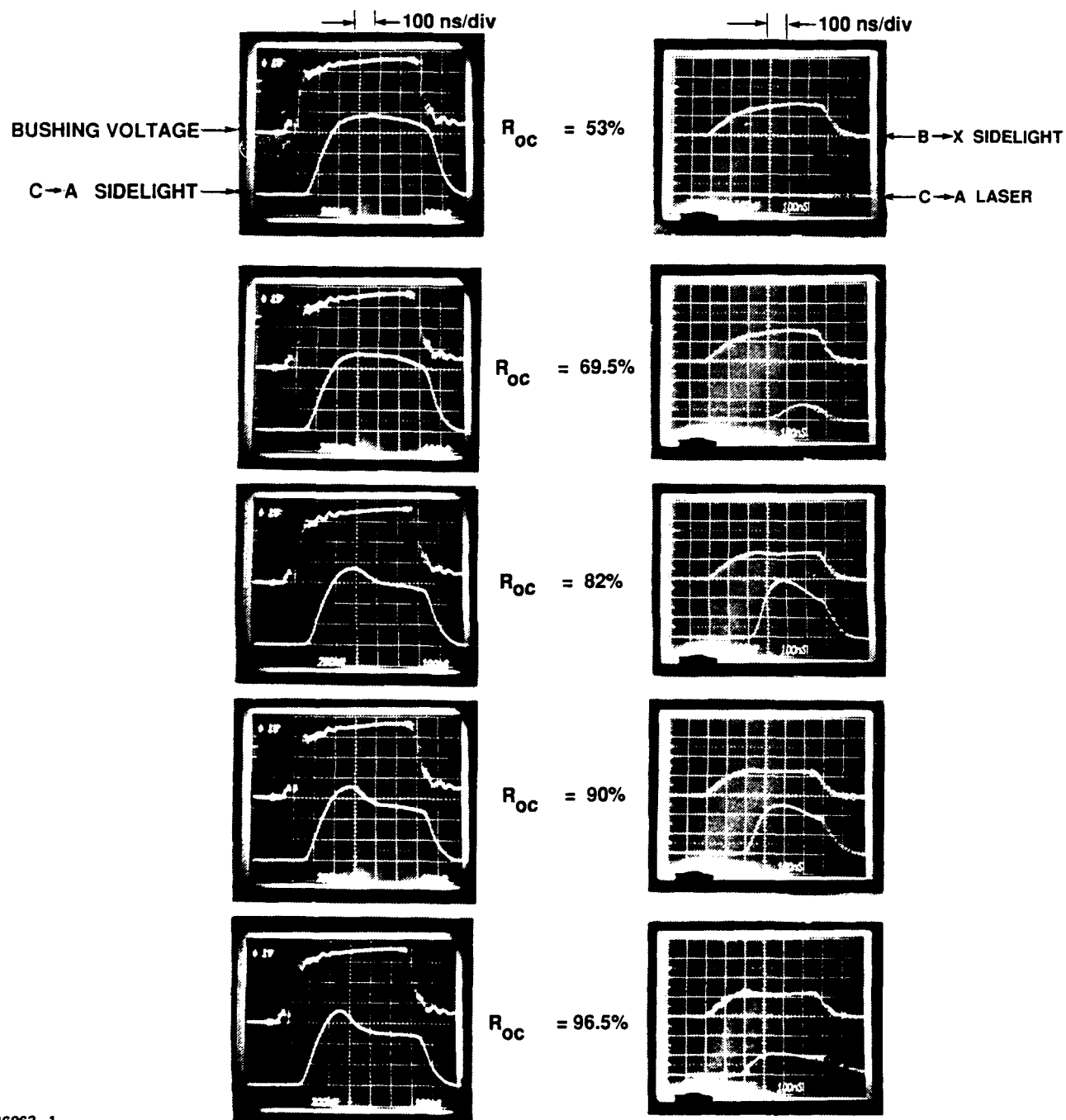
prior to injection.<sup>3</sup> Even so, there was a significant delay in the laser turn-on time due to the fact that a substantial amount of time was required for the intracavity flux to build up to saturation levels from noise. The observed delay was consistent with measurements of the small-signal net gain. The delay was subsequently reduced by injecting radiation from an external source, and this yielded significantly higher laser output energy and higher efficiency. This is discussed in greater detail in Sec. 7.0.

Figure 8 shows the laser and sidelight temporal characteristics for some other output coupler reflectivities. As expected, the amount of sidelight suppression increased as the reflectivity was increased, and the time required to establish laser oscillations decreased. Sidelight suppression occurred only after laser oscillations had become established. At high mirror reflectivity, laser emission continued for a short time after the termination of the e-beam pulse, due to the fact that light was trapped within the laser cavity and could only leak out slowly.

Figure 9 shows the temporal characteristics at various partial pressures of  $\text{NF}_3$ . While the  $\text{XeF}(\text{C} \rightarrow \text{A})$  sidelight fluorescence intensity was greatest at a partial pressure of 1 Torr, the laser output decayed very rapidly during the pulse. Higher partial pressures of  $\text{NF}_3$  were needed to attain more constant laser output during the pulse.  $\text{NF}_3$  is an effective electron attacher at electron energies above 1 eV. Apparently, it must be present in sufficiently high quantities to limit the increase in electron density during the e-beam pulse and the buildup of excited atomic rare-gas photoabsorbers.

### 3.5 SPECTRAL CHARACTERISTICS

The free-running laser output spectrum is shown, together with the unsuppressed sidelight fluorescence spectrum, in Fig. 10. The spectrometer resolution was approximately 2 nm, with a 300 line/mm grating, during these measurements. Figure 11 shows the free-running laser spectrum at a higher instrument resolution of 1.3 Å, achieved with a 2400 line/mm grating. The spectral modulation is deeper, and the wavelengths of the peaks and valleys have been identified. Sidelight radiation was routed to the entrance slit of the grating spectrometer through a periscope-type arrangement, consisting of a hollow tube that was lined internally with aluminum-coated Kapton foil. Under free-running conditions the laser spectrum was 16 nm (160 Å) wide (FWHM) and



N6963-1

Figure 8. Temporal characteristics for varying output coupler reflectivity under free-running conditions.

# PARTIAL PRESSURES

F<sub>2</sub> 1 TORR  
 Xe 8 TORR  
 Kr 300 TORR  
 Ar 1635 TORR  
 REFLECTIVITY 86.5%

$P(NF_3) = 5 \text{ TORR}$

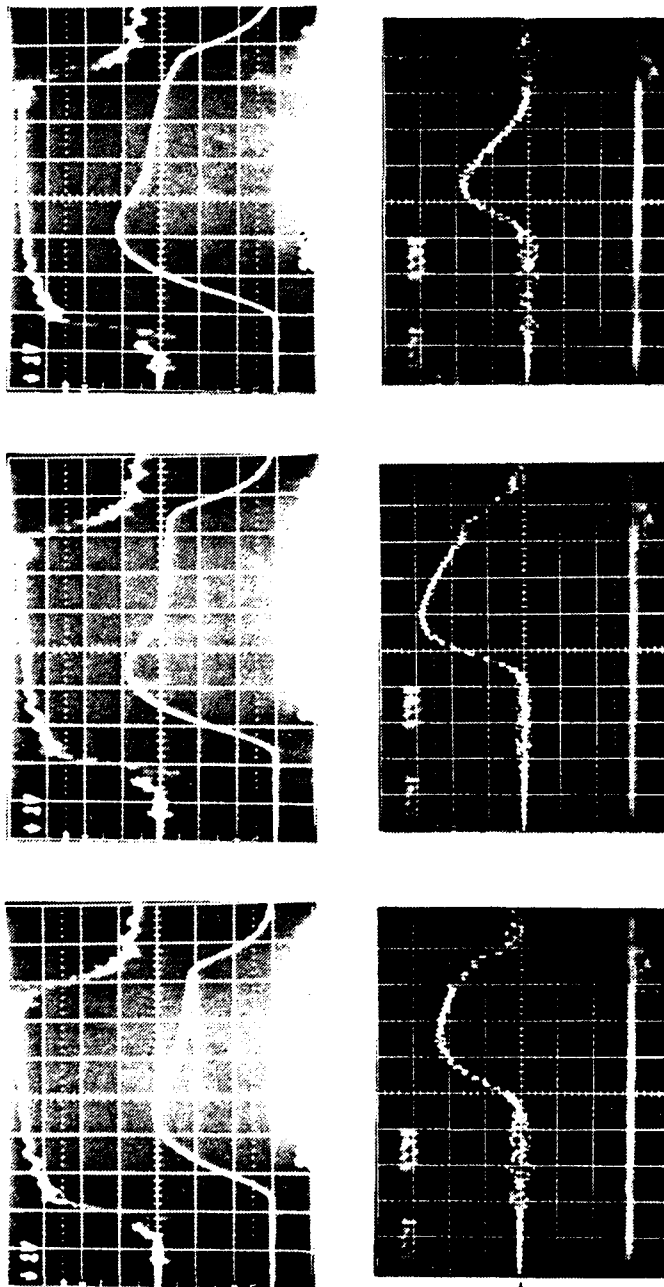
$P(NF_3) = 2 \text{ TORR}$

$P(NF_3) = 1 \text{ TORR}$

BUSHING VOLTAGE →

SUPPRESSED  
 C→A SIDELIGHT →

C→A LASER →



100 ns/div

N6984-1

Figure 9. Temporal characteristics for varying  $NF_3$  partial pressure under free-running conditions.

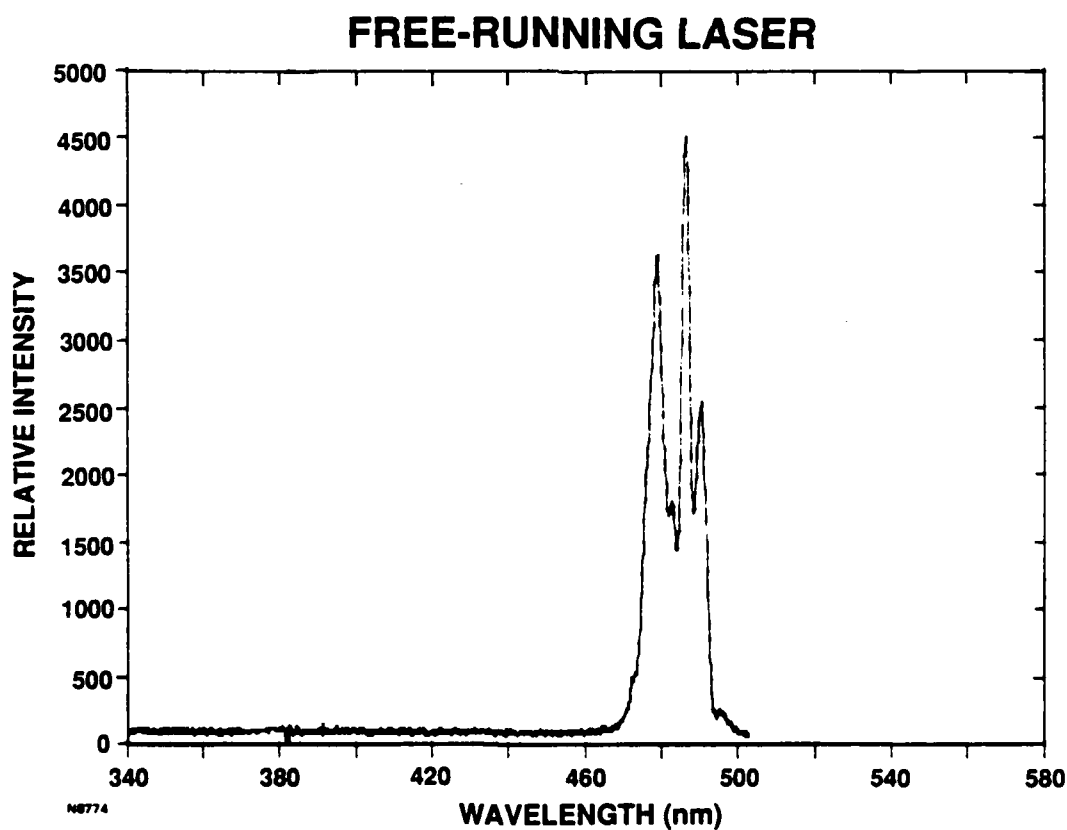
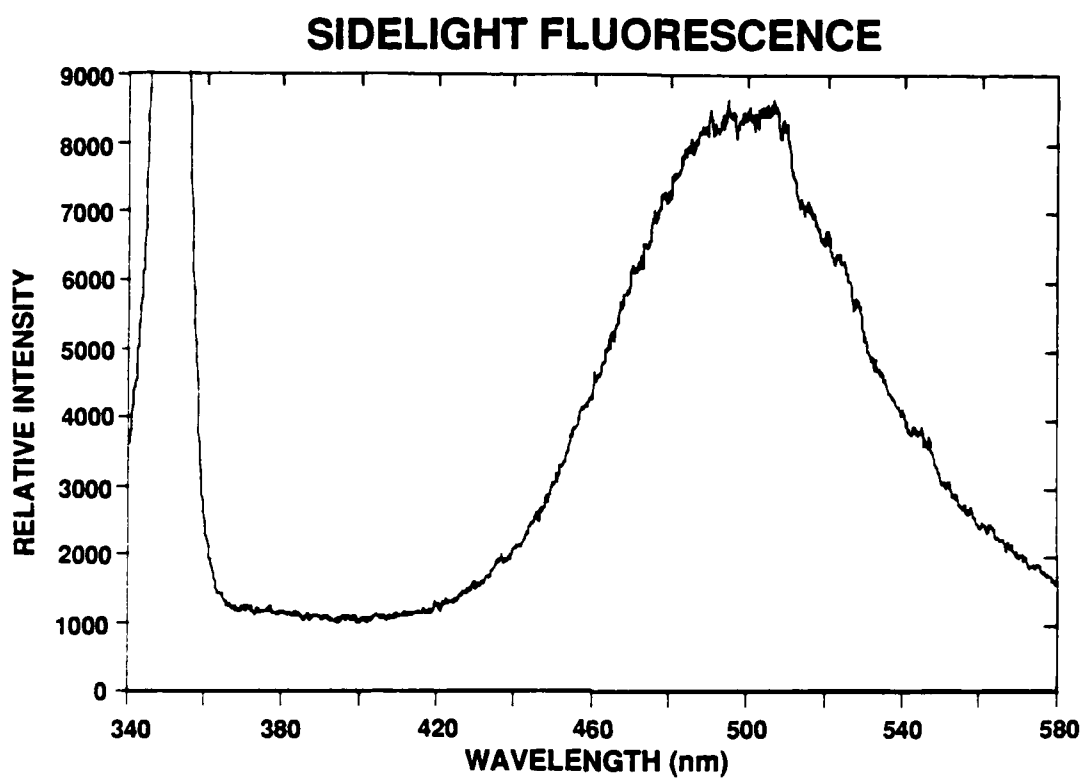


Figure 10. Spectrum of unsuppressed sidelight fluorescence and of free-running laser output. Instrumental resolution was 2 nm.

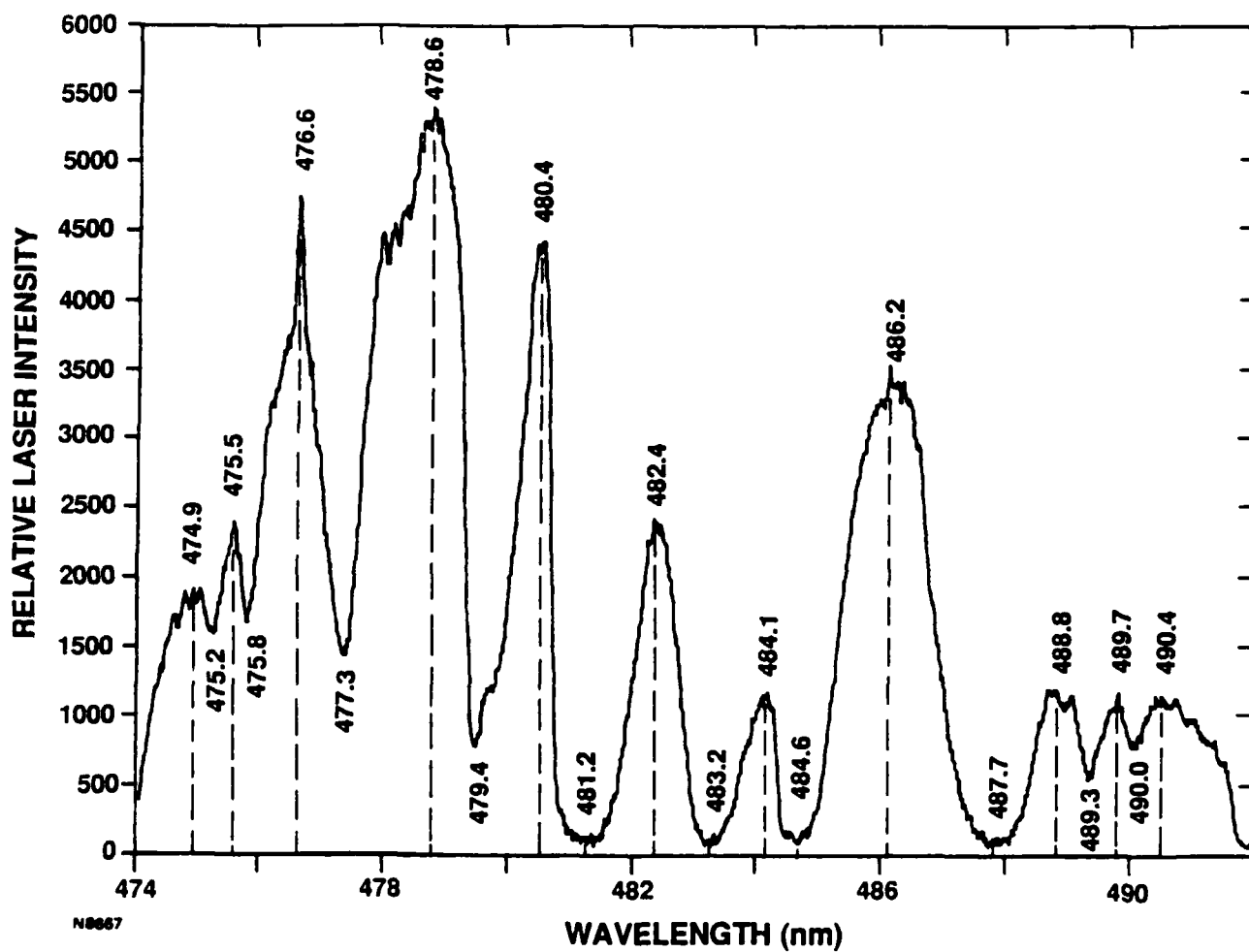


Figure 11. Free-running laser spectrum at instrumental resolution of 0.13 nm (1.3 Å).

was centered near 483 nm. The fluorescence spectrum was broader, providing an indication of the wide tunability of this laser system.

The structure observed in the free-running laser spectrum had previously been seen at high pump rate<sup>7,8</sup> and is believed to be due to discrete, narrowband absorption by excited rare-gas atomic species.<sup>9</sup> While XeF(B→X) laser emission was not observed in any of the experiments at low pump rate, the sidelight fluorescence spectrum did show both XeF(B→X) and XeF(C→A) emissions. The XeF(C→A) fluorescence spectrum peaked at slightly longer wavelengths than the laser spectrum. This is in contrast to previous work at high pump rate and high gas pressure where the opposite was the case.<sup>1</sup> A similar fluorescence spectrum was observed when a Schott GG375 filter was placed in front of the spectrometer to prevent possible contributions from KrF(B→X) emission at 249 nm in second order, and also when neon was substituted for the argon buffer. The spectrum also did not change significantly when the partial pressure of krypton was varied. Figures 12 and 13 show sidelight fluorescence spectra for varying amounts of krypton, with neon and argon as the buffer gases, respectively. In each case the buffer partial pressure was adjusted to maintain the same total e-beam stopping power and, hence, approximately the same specific energy input.

Fluorescence spectra have also been recorded without xenon, and without either xenon or krypton. The results are presented in Fig. 14. The peak at 380 nm without xenon is probably due to Kr<sub>2</sub>F which is ordinarily quenched by xenon. The fluorescence below 340 nm, observed without xenon and krypton, is probably due to Ar<sub>2</sub>F.

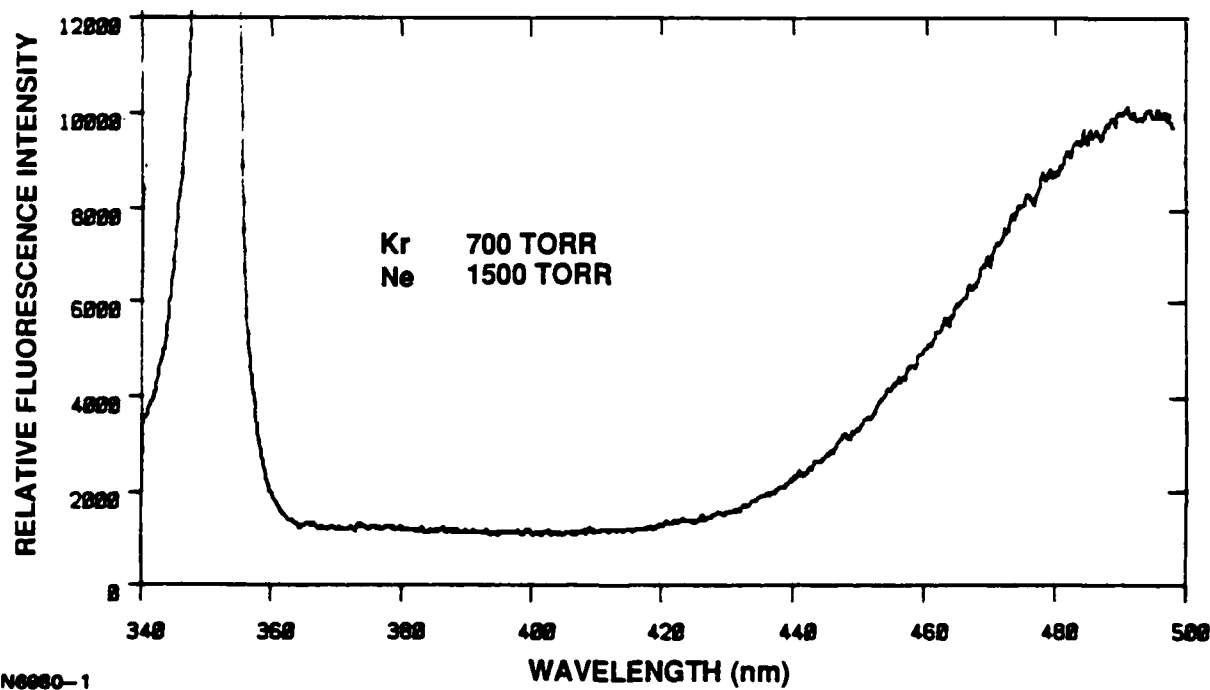
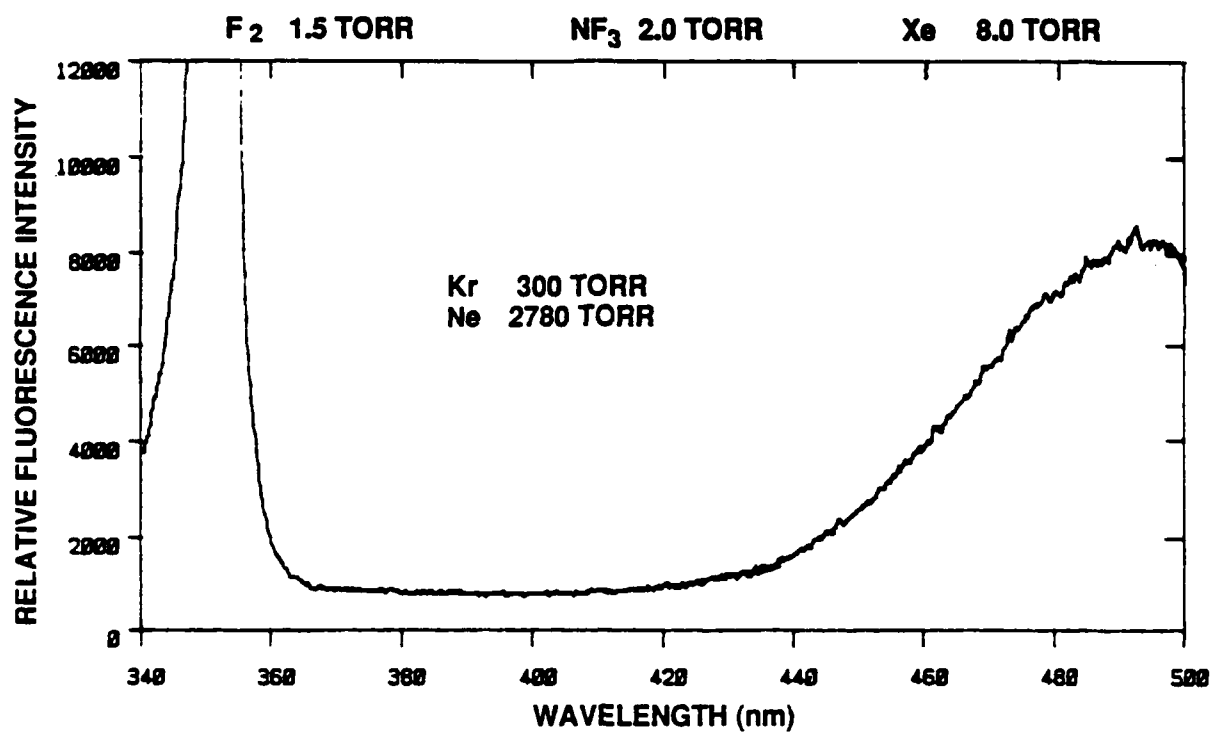
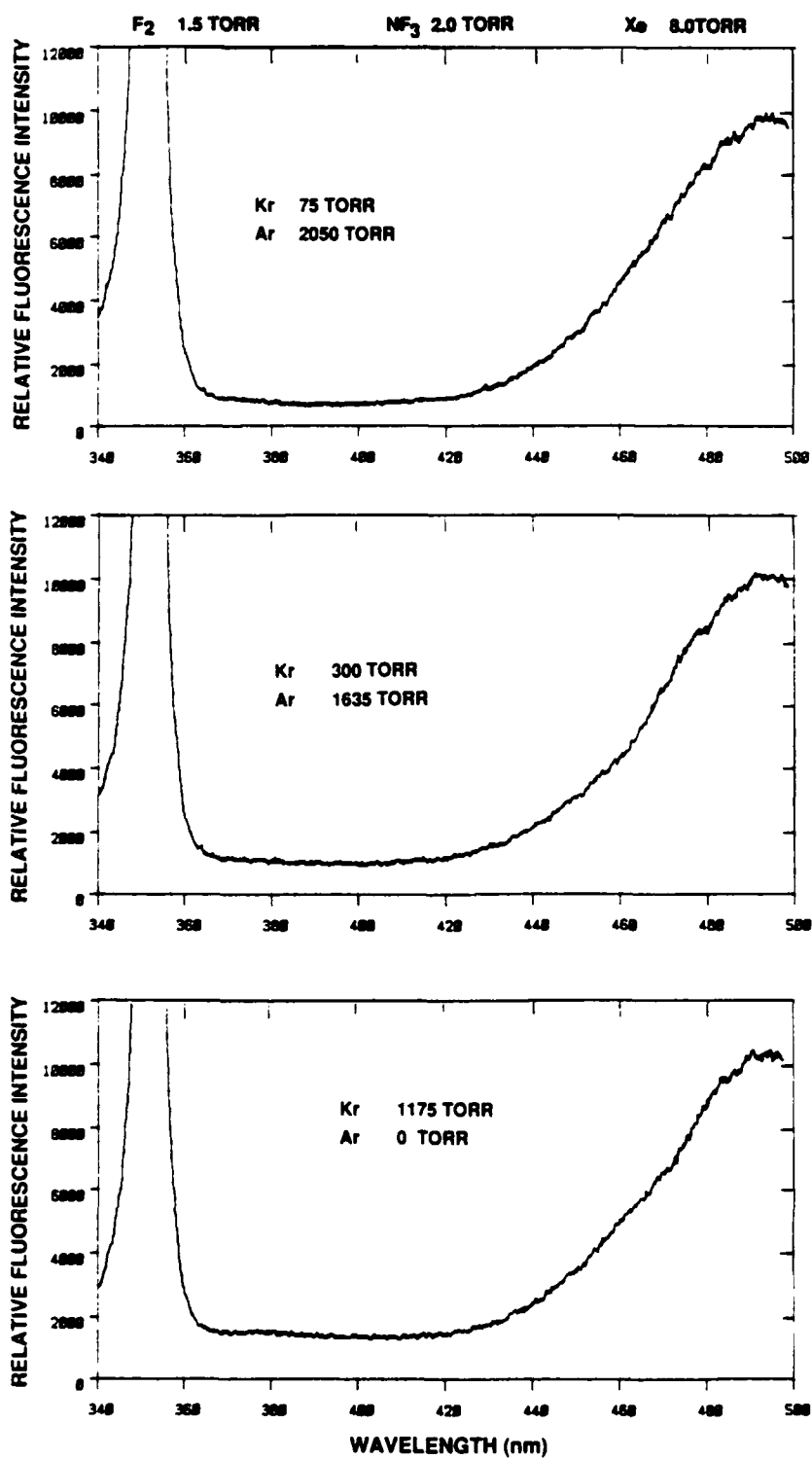


Figure 12. Unsuppressed sidelight fluorescence spectra for neon buffer and varying krypton partial pressure.



N6982-1

Figure 13. Unsuppressed sidelight fluorescence spectra for argon buffer and varying krypton partial pressure.

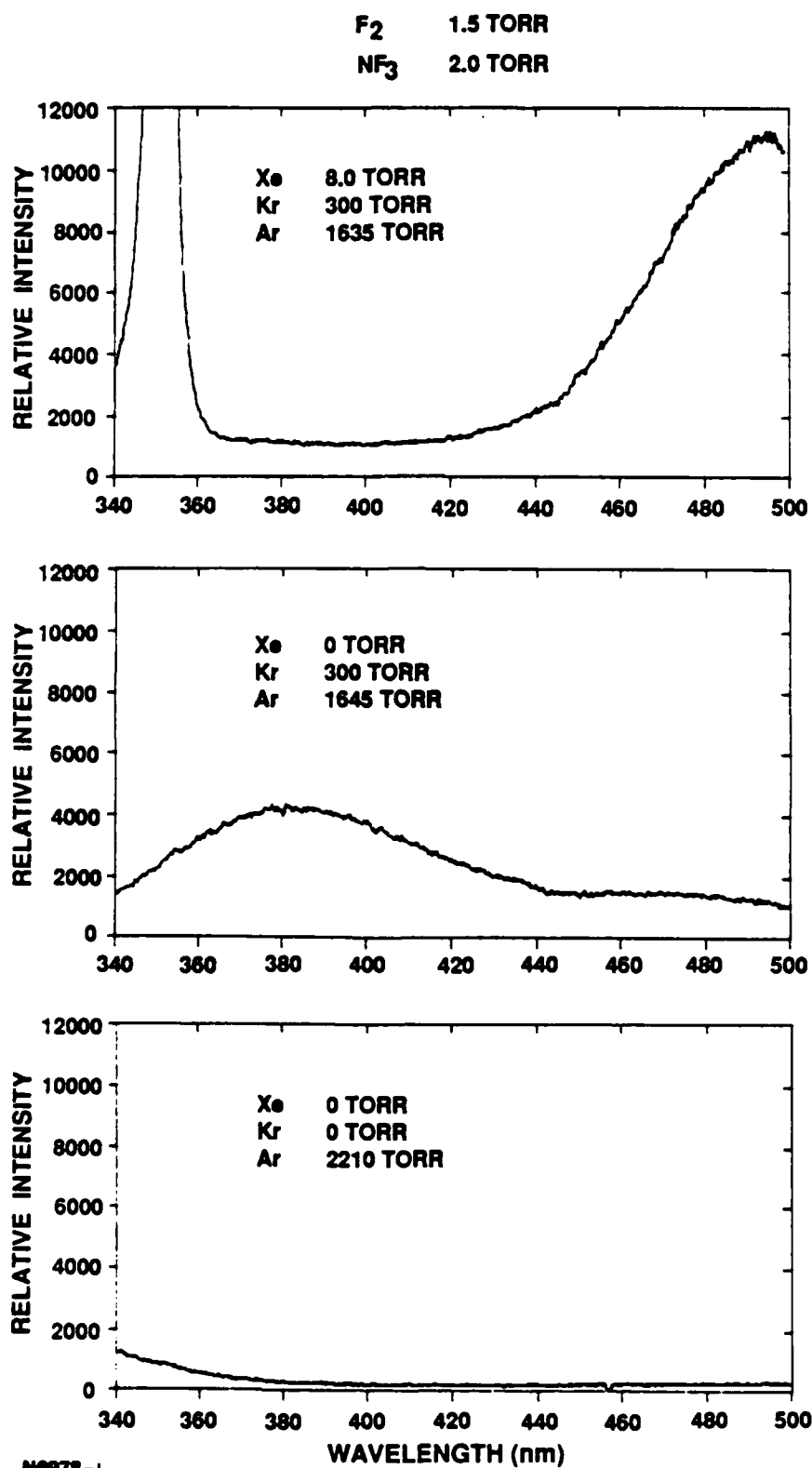


Figure 14. Unsuppressed sidelight fluorescence spectra with and without xenon and krypton.

#### 4.0 OTHER LASER GAS MIXTURES

In an attempt to improve the performance of the free-running XeF(C→A) laser further, prior to injection, other carefully selected gases were tested as part of the laser gas mixture, either as additives or as substitutes for gases already present. As previously discussed, in one such experiment a portion of the argon buffer (135 Torr) was replaced with a much larger quantity of helium (1000 Torr) to limit the temperature rise associated with e-beam heating of the gas. This led to a 30% decline in the laser output energy rather than the hoped-for increase. The XeF(B→X) and XeF(C→A) sidelight fluorescence signals also declined by 10-15 percent.

In a second experiment the entire quantity of argon gas (1635 Torr) was replaced with an equivalent (in terms of e-beam stopping power) amount of neon (2780 Torr). Neon has several features which make it potentially attractive as a buffer gas. These include a fast sound speed, which ensures rapid acoustic clearing in a repetitively pulsed device, and a relatively low Gladstone-Dale coefficient, which relaxes the requirements on medium homogeneity in a device capable of producing a high quality output beam. However, with neon as the buffer, lasing failed to occur, and the XeF(C→A) sidelight fluorescence signal decreased by approximately 25 percent. Table 3 provides a list of transfer rate constants for gases of interest. As can be seen in this table, the XeF(B)→XeF(C) transfer rate constant  $k_{BC}$  is nearly an order of magnitude smaller for neon than for argon. To ensure an overall rate of population transfer similar to that for the argon-buffered mixture (i.e., approximately  $8 \times 10^8 \text{ s}^{-1}$ , equivalent to a transfer time of 1.2 ns which is short relative to the B-state radiative lifetime of 13.5 ns), additional krypton was subsequently added to the neon-buffered mixture. The amount of neon was simultaneously reduced to maintain the same total e-beam stopping power. In particular, a gas mixture containing 700 Torr of krypton and 1500 Torr of neon was tested. The increase in krypton partial pressure did lead to a significant increase in the XeF(C→A) sidelight fluorescence signal with neon and to lasing late in the 600-ns e-beam excitation pulse, but the intrinsic (energy) efficiency was still only 0.09%, which was well below the efficiency achieved with argon. The sidelight fluorescence and laser output signals recorded with neon as the buffer are presented in Fig. 15.

TABLE 3. XeF(B)→XeF(C) TRANSFER RATE CONSTANT  $k_{BC}$ <sup>a</sup>

	$k_{BC}$ ( $10^{-12}$ cm <sup>3</sup> molecule <sup>-1</sup> s <sup>-1</sup> )
Ne	1.0 (± 0.2)
He	3.1 (± 0.3)
Ar	8.6 (± 1.1)
Kr	34 (± 3)
CF <sub>4</sub>	41 (± 4)
N <sub>2</sub>	44 (± 6)
F <sub>2</sub>	50 (± 30)
Xe	61 (± 13)
NF <sub>3</sub>	83 (± 20)

<sup>a</sup>From Ref. 10.

PARTIAL PRESSURES  
 F<sub>2</sub> 1.5 TORR  
 NF<sub>3</sub> 2.0 TORR  
 Xe 8.0 TORR  
 REFLECTIVITY 86.5%

Kr 300 TORR  
 Ne 2780 TORR

Kr 700 TORR  
 Ne 1500 TORR

BUSHING VOLTAGE

C → A SIDELIGHT\*

B → X SIDELIGHT\*

C → A LASER

100 ns/div

N6979-1

\* NEGLIGIBLE SUPPRESSION

$\eta_{INT} = 0\%$

$\eta_{INT} = 0.09\%$

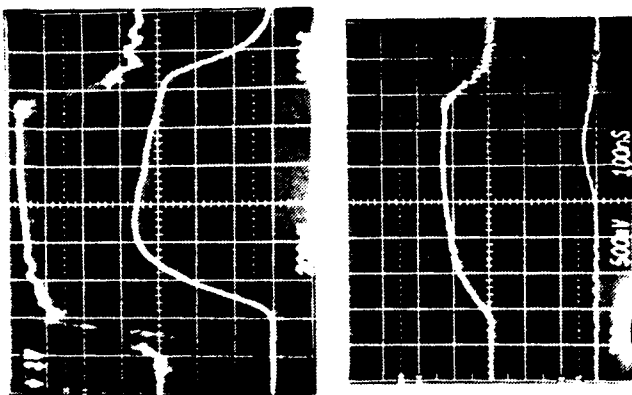


Figure 15. Temporal characteristics for neon buffer and varying krypton partial pressure, under free-running conditions.

In the next round of experiments an attempt was made to substitute nitrogen for krypton in the five-component gas mixture. Nitrogen has a higher  $\text{XeF(B)} \rightarrow \text{XeF(C)}$  transfer rate constant than krypton (see Table 3), and it is considerably less expensive. Nitrogen was tested with both argon and neon as buffer gases. In both cases the partial pressures of nitrogen and the buffer gas were adjusted to maintain the same total e-beam stopping power and approximately the same e-beam energy input. The gas combinations that were tested were 1) 250 Torr of nitrogen with 1970 Torr of argon, and 2) 610 Torr of nitrogen with 3235 Torr of neon. In both cases the overall  $\text{XeF(B)} \rightarrow \text{XeF(C)}$  transfer rate was higher than that for the standard, krypton-containing mixture, which was desirable. (The  $\text{F}_2$ ,  $\text{NF}_3$  and xenon partial pressures were 1.5, 2 and 8 Torr, respectively, as in other experiments.)

Unfortunately, the substitution of nitrogen for krypton led to significant declines in the  $\text{XeF(B)} \rightarrow \text{X}$  and  $\text{XeF(C)} \rightarrow \text{A}$  sidelight fluorescence signals (by a factor of the order of four) and to the complete cessation of  $\text{XeF(C)} \rightarrow \text{A}$  lasing.

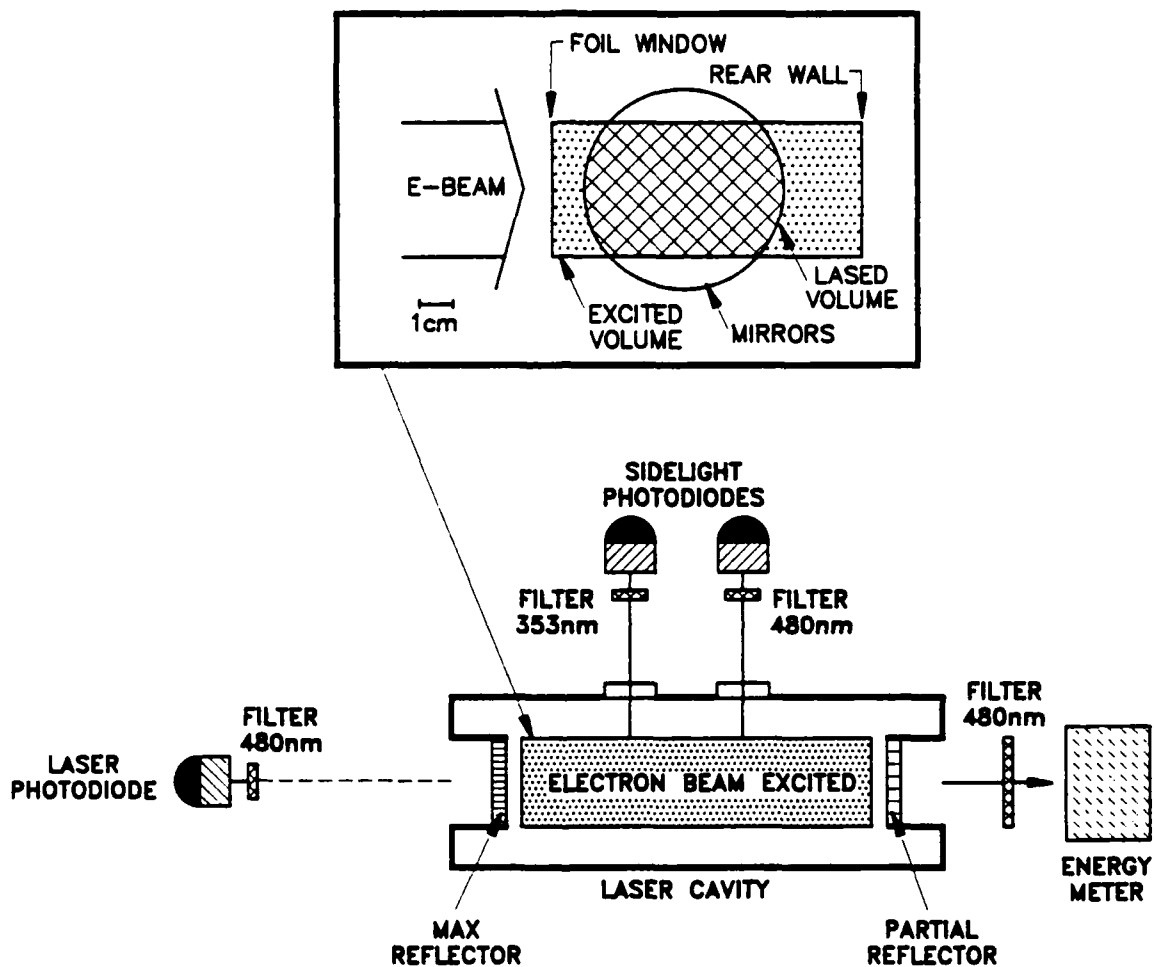
The final change that was tested was the addition of varying amounts of  $\text{CF}_4$  to the gas mixture. The gas  $\text{CF}_4$  can serve as a halogen donor, and it also possesses an  $\text{XeF(B)} \rightarrow \text{XeF(C)}$  transfer rate constant which is higher than that of krypton. (See Table 2.) In the first such set of experiments, partial pressures of 2 and 20 Torr of  $\text{CF}_4$  were added to the standard five-component mixture listed in Table 2. In a subsequent experiment the 300 Torr of krypton were replaced with 250 Torr of  $\text{CF}_4$ , and the argon partial pressure was reduced slightly to 1530 Torr. While a modest amount of lasing was observed with 2 Torr of  $\text{CF}_4$  added to the standard mixture (intrinsic efficiency of 0.75%), no lasing was observed with either 20 or 250 Torr of  $\text{CF}_4$ . Both sidelight fluorescence signals showed a monotonic decline in amplitude with increasing  $\text{CF}_4$ . In conclusion, the five-component laser gas mixture listed in Table 2 is the best combination of gases identified thus far.

## 5.0 MAXIMUM ENERGY EXTRACTION EXPERIMENT

To increase the amount of laser energy extracted from the device, the apparatus was subsequently outfitted with larger diameter mirrors and the mask at the laser output was removed. The 2-in.-diameter mirrors were replaced with 3-in.-diameter mirrors which had a clear aperture of 5.8 cm. (The 3-in.-mirrors were spaced by 112.5 cm.) During this experiment it was convenient to extract the energy from the opposite end of the cavity, and laser temporal characteristics were recorded with a photodiode which was mounted behind the slightly transmitting maximum reflector. Figure 16 shows the experimental setup and the region from which laser energy was extracted.

A total of 4 J of energy was extracted from the free-running device with the larger diameter mirrors in place. The inferred intrinsic efficiency was similar to that obtained with the 2-in.-diameter mirrors and mask present, proving that the inferred efficiency is independent of the physical size of the extraction volume and of the sampled volume, as required.

The corresponding temporal characteristics are shown in Fig. 17. As before, the laser turned on late. The amount of sidelight suppression was larger, due to the fact that more of the collected sidelight came from regions which had seen intracavity flux. Table 4 summarizes the results obtained during this and the previous free-running experiments.



P1248

Figure 16. Schematic diagram of experimental setup for maximum energy extraction. Inset shows an end-on view of the laser cavity (to scale).

REFLECTIVITY 87%

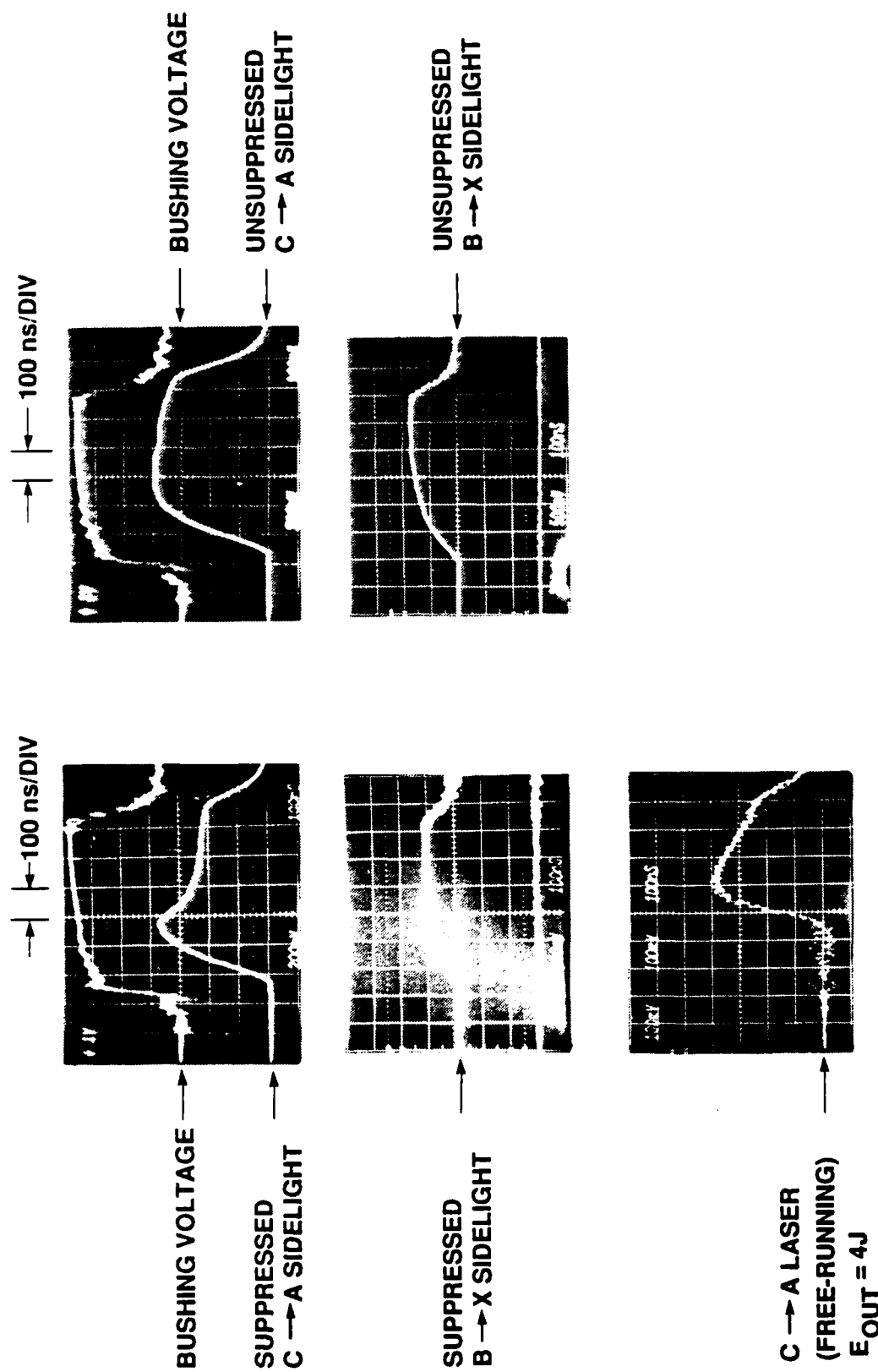


Figure 17. Temporal pulse shapes for free-running oscillator with 3-in.-diameter mirrors (left side) and without laser oscillation (right side).

N8661 - 1

TABLE 4. SUMMARY OF FREE-RUNNING OSCILLATOR RESULTS

Intrinsic efficiency	1.1%
Output energy	4.0 J
Specific output energy	2.0 J/liter
Laser pulse duration	350 ns
Laser bandwidth	160 Å

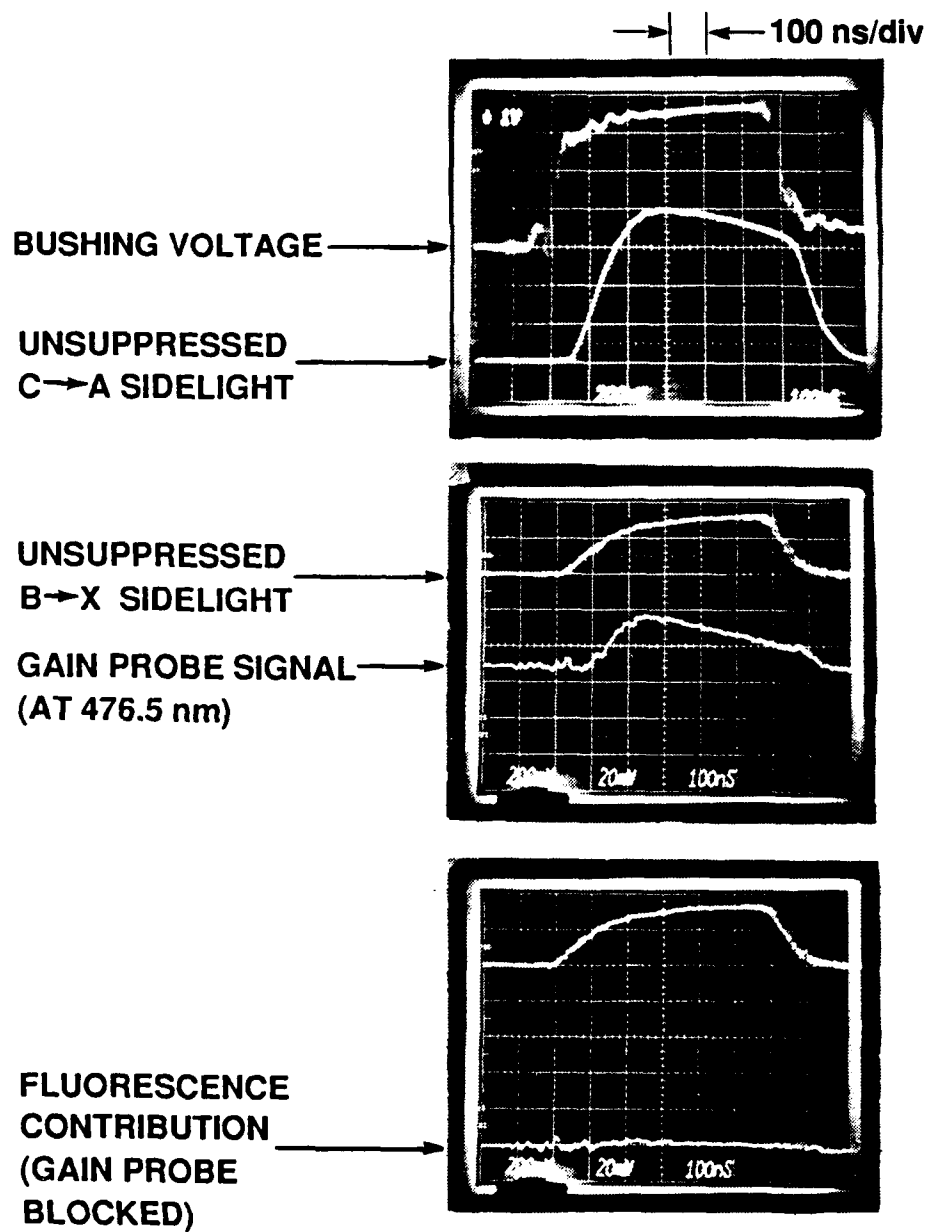
## 6.0 SMALL-SIGNAL NET GAIN MEASUREMENTS

Time resolved measurements of the small-signal net gain (i.e., gain minus absorption) were made by passing a probe laser beam from a CW argon-ion laser through the excited medium. The beam was passed through the centers of the 2-in.-diameter uncoated windows which replaced the resonator mirrors. The probe laser was tuned to various wavelengths across the XeF(C $\rightarrow$ A) gain profile.

Figure 18 shows an example of the raw data. The probe signal amplitude increased when the medium was excited. The linearity of the photodiode response was verified, and a shot was taken with the probe beam blocked to determine the contribution of fluorescence to the photodiode signal. The fluorescent contribution was minimized by locating the photodetector as far from the excited medium as possible, and by mounting masks at intermediate locations. The XeF(B $\rightarrow$ X) contribution was rejected with a Schott GG385 filter.

Figure 19 shows the gain as a function of time during the e-beam pulse at eight different wavelengths. In each case the gain declined during the e-beam pulse, following the attainment of a peak value. The rate of decline, which generally was larger at the shorter wavelengths, exceeded the rate of decline of the unsuppressed XeF(C $\rightarrow$ A) sidelight fluorescence signal (see Fig. 7), suggesting that a part of the decline in the net gain was due to an increase in photoabsorption.

The peak gain, the gain just prior to e-beam pulse termination and the temporally averaged gain are all plotted as a function of wavelength in Fig. 20. The gain profile was found to be centered around 485 nm during much of the pulse, but it shifted slightly toward longer wavelengths late in the pulse. The maximum peak gain was 0.4%/cm.



N6935

Figure 18. Temporal waveforms during small-signal net gain measurement at 476.5 nm.

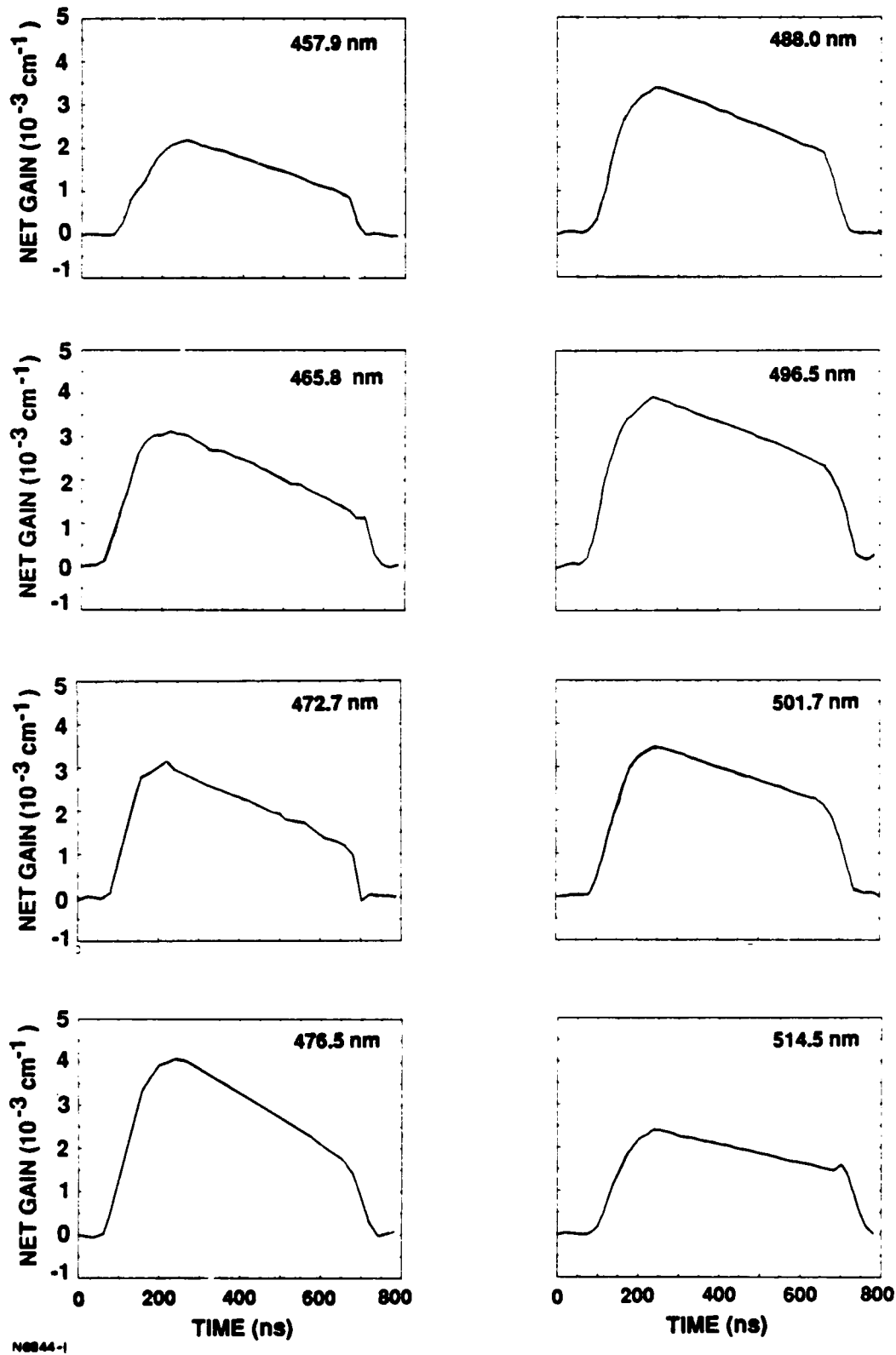
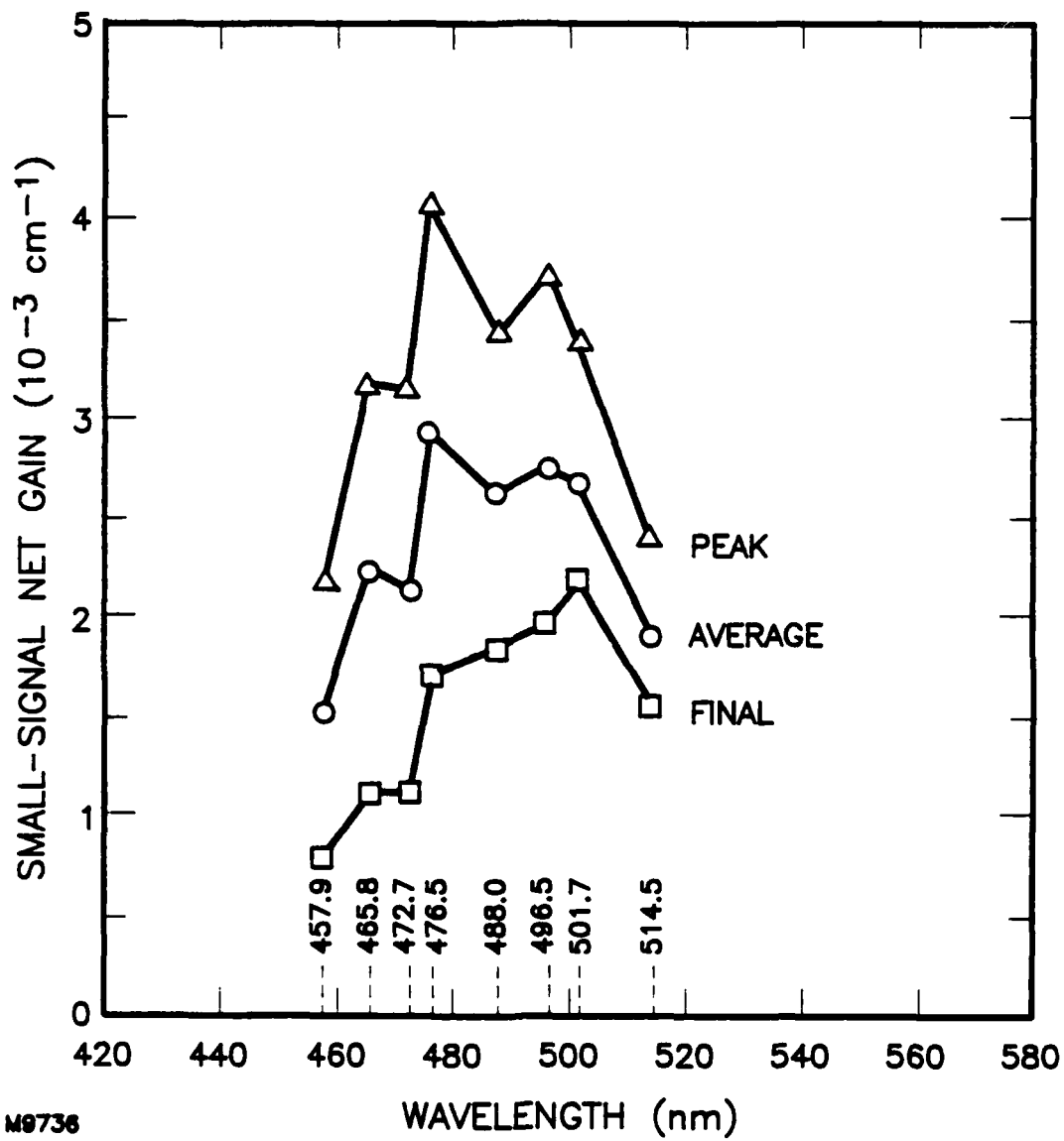


Figure 19. Small-signal net gain as a function of time during e-beam pulse, at varying wavelength.



M9736

Figure 20. Small-signal net gain as a function of wavelength.

## 7.0 INJECTION-CONTROLLED OSCILLATOR EXPERIMENTS

Subsequent to the free-running oscillator experiments and small-signal net gain measurements, a series of injection-controlled oscillator experiments were performed. The objectives were to 1) demonstrate improved energy extraction due to faster laser turn-on, 2) demonstrate a substantial reduction in laser bandwidth, and 3) show wavelength tuning.

### 7.1 EXPERIMENTAL SETUP

Figure 21 shows a schematic diagram of the setup which was used in these experiments. A stable cavity identical to that utilized in the free-running experiments was used. The cavity was injected with collimated light from a long-pulse ( $\geq 600$  ns FWHM), coaxial, flashlamp-pumped dye laser (Candela SLL-500). The dye laser, which was operated with Exciton Coumarin 480 dye, was outfitted with a triple-prism tuner to reduce the dye laser bandwidth to less than 1.3 Å, the resolution of the spectrometer.

The beam was injected into the XeF(C $\rightarrow$ A) cavity through a Glan-air polarizing prism and a Fresnel rhomb. The Glan-air polarizer was oriented to transmit the linearly polarized dye laser beam. The rhomb was oriented with the diagonal at 45° relative to the incident electric vector, so as to produce equal s- and p-polarization components at the reflecting faces of the rhomb. The rhomb introduced a quarter-wave shift between the s- and p-polarization components, yielding circularly polarized light at the exit. Oscillations within the XeF(C $\rightarrow$ A) cavity which were controlled by this injected light were, therefore, circularly polarized. The output XeF(C $\rightarrow$ A) laser radiation was circularly polarized in the opposite sense from the injected light, due to propagation in the opposite direction. The rhomb introduced a quarter-wave shift into the XeF(C $\rightarrow$ A) output beam, turning the circularly polarized radiation back into linearly polarized light. The plane of polarization of this light was rotated by 90° relative to the dye laser light. Consequently, the injection-controlled XeF(C $\rightarrow$ A) light was not transmitted through the polarizer but rather was reflected by the polarizer onto a new, orthogonal path where it was analyzed in terms of energy, and spectral and temporal characteristics. This isolated the dye laser from the XeF(C $\rightarrow$ A) laser output. Dye laser radiation which was reflected off of the XeF(C $\rightarrow$ A) laser mirrors was

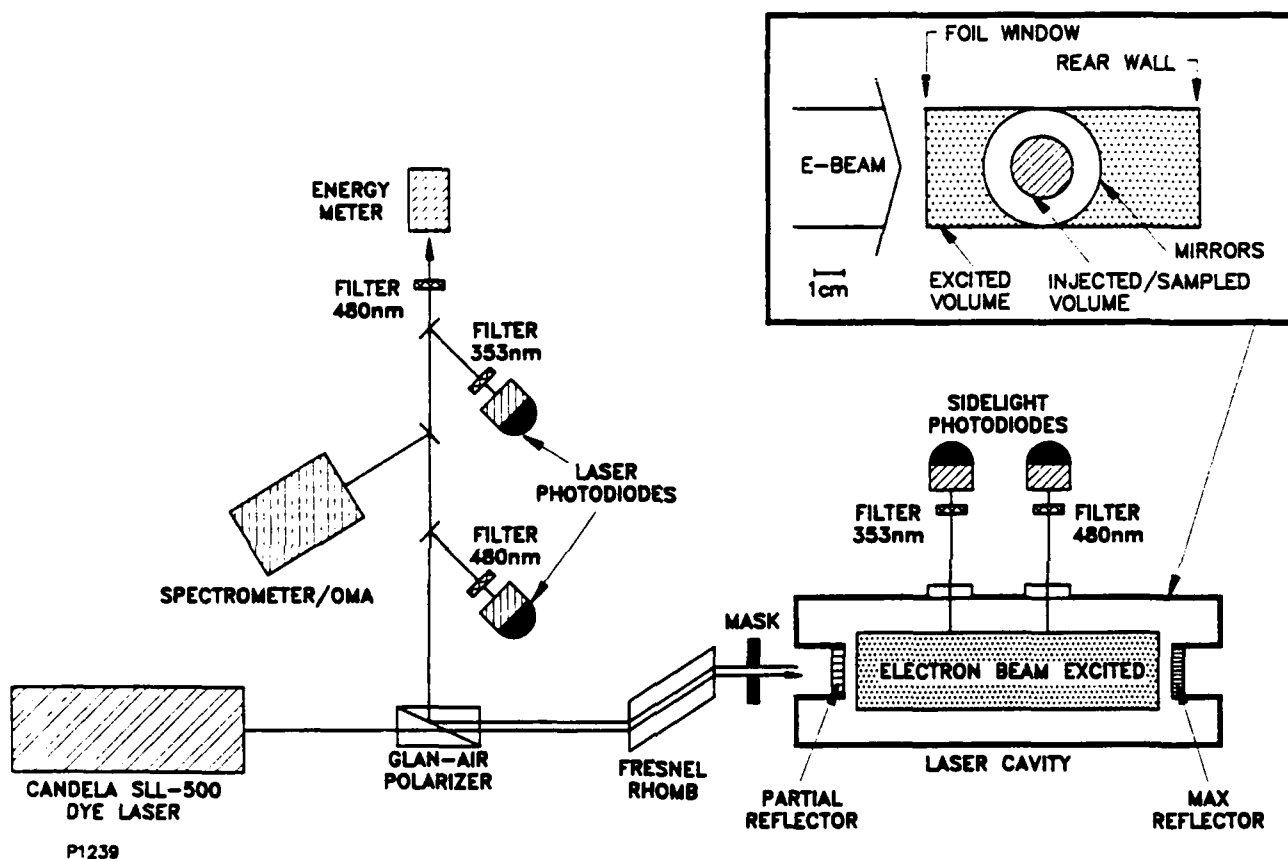


Figure 21. Schematic diagram of setup for injection-controlled oscillator experiments. Inset shows an end-on view of the laser cavity (to scale).

also directed onto this orthogonal path by the Glan-air polarizer, and this served to isolate the dye laser from feedback from the XeF(C→A) laser mirrors. The contribution of the dye laser radiation to signals observed within the diagnostic arm was small ( $< 10\%$ ) and correctable.

The laser cavity was outfitted with 2-in.-diameter mirrors during these experiments, which permitted lasing over a 3.8-cm-diameter region. However, as was the case during most of the free-running experiments, a mask was placed at the output of the XeF(C→A) laser to select a uniformly pumped region and to define the sampled volume. A 1-to-2 beam expanding telescope was placed between the rhomb and this mask (not shown in Fig. 21) to expand the injected laser beam to the dimensions of this aperture. A 2-cm-diameter, circular aperture, consistent with the circular geometry of the dye laser beam, was chosen.

The XeF(C→A) laser cavity was aligned using a Davidson Optronics alignment telescope. The dye laser beam was then aligned relative to the XeF(C→A) cavity by using an argon-ion alignment laser. The argon-ion beam was also utilized to verify that the Glan-air polarizer and Fresnel rhomb were correctly oriented for good isolation.

The partially reflecting output mirror of the XeF(C→A) laser cavity through which light was injected had a reflectivity of 82%. The power density of the dye laser beam which was incident upon this mirror was approximately  $5 \times 10^4 \text{ W/cm}^2$ , and the power density injected into the cavity was of the order of  $1 \times 10^4 \text{ W/cm}^2$ .

## 7.2 TEMPORAL CHARACTERISTICS

Figure 22 shows the temporal characteristics of the injected dye laser beam and of the injection-controlled XeF(C→A) laser output (right-hand set of oscillographs). The injected beam was monitored with a photodiode placed behind a slightly transmitting fold mirror in the injection arm (not shown in Fig. 21). The dye laser which was tuned to a peak in the free-running laser spectrum at 486.2 nm, was timed so that the XeF(C→A) cavity was filled with injected radiation before the e-beam was fired and the gain began to rise. The XeF(C→A) laser cavity was injected throughout the e-beam pulse.

The left-hand set of oscillographs in Fig. 22 show the case where the XeF(C→A) laser cavity was not injected but instead was allowed to free run.

# REFLECTIVITY 82%

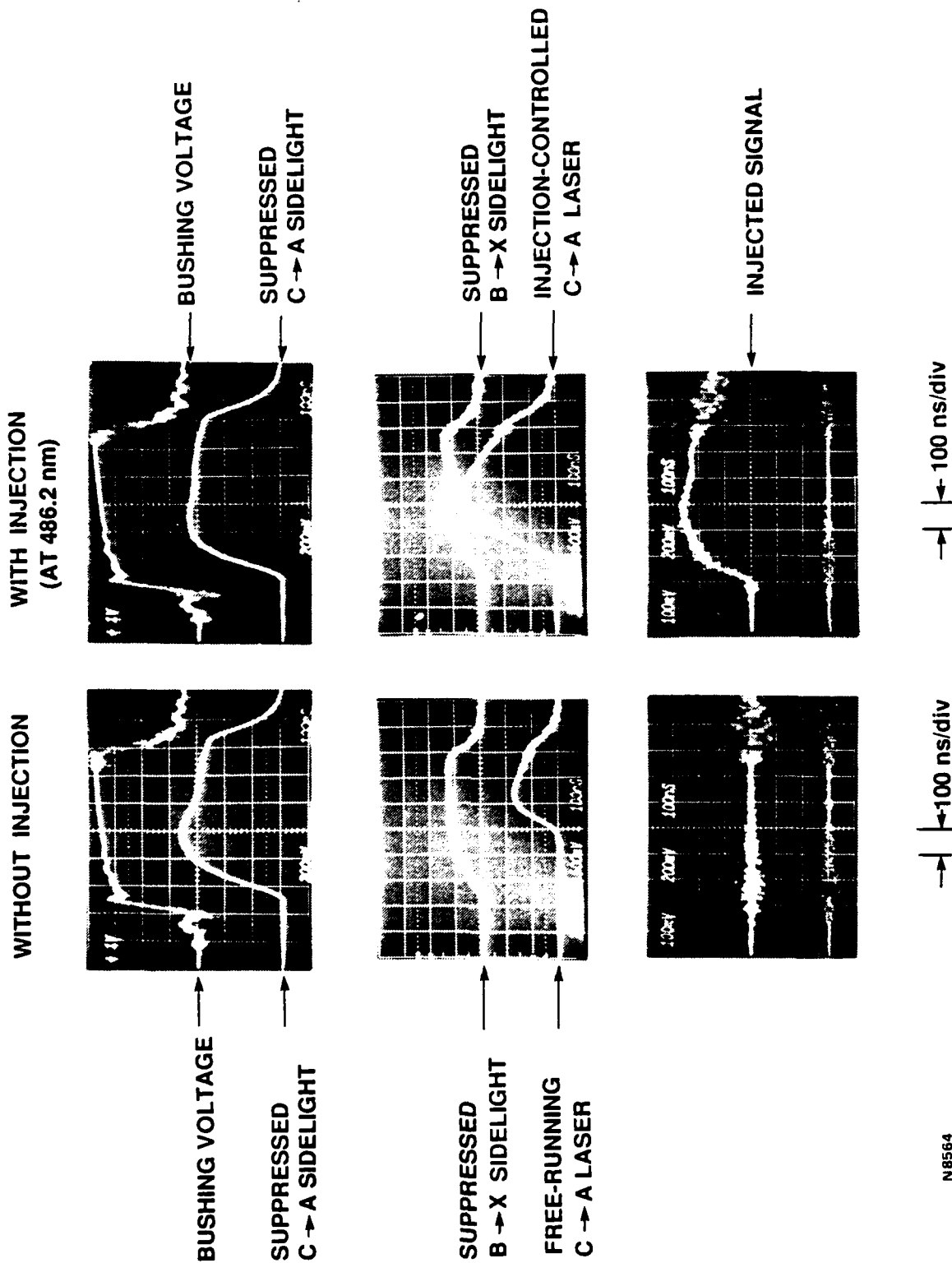
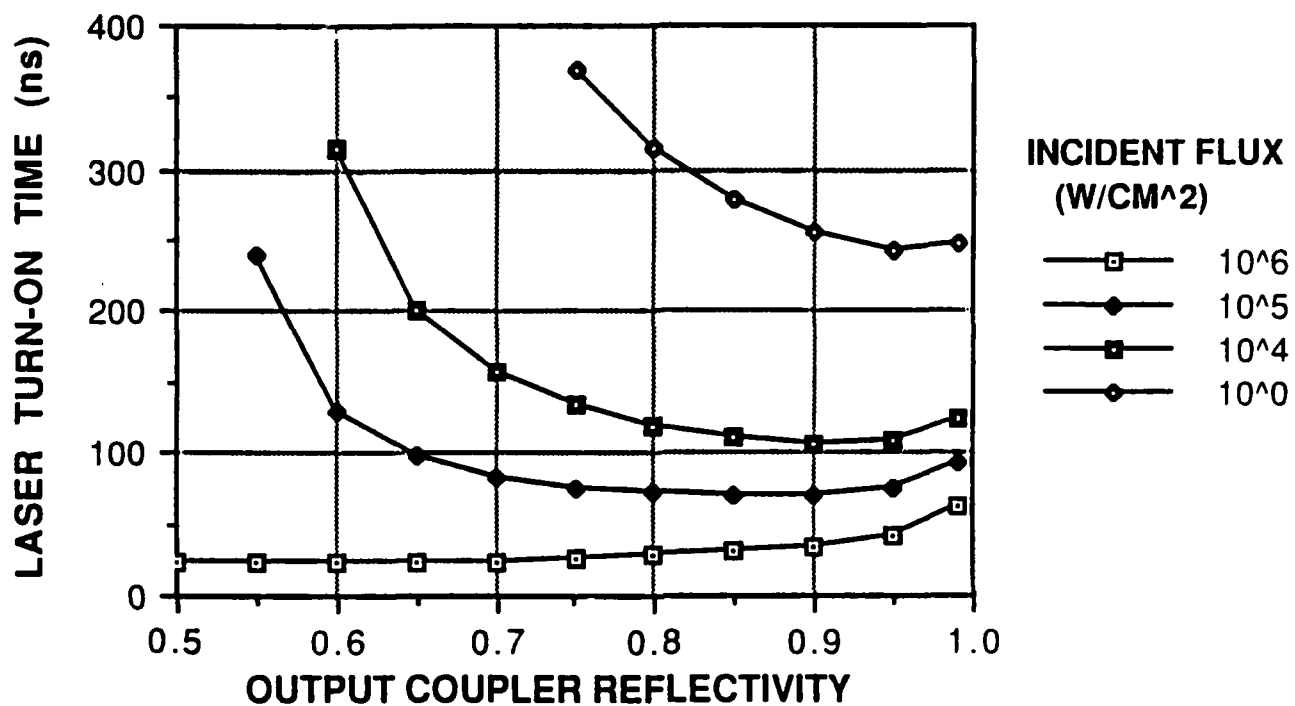


Figure 22. Temporal pulse shapes for free-running oscillator (left side) and injection-controlled oscillator (right side). Note the earlier laser turn-on with injection.

As in previous experiments, the free-running XeF(C→A) laser output was significantly delayed relative to the start of e-beam pumping, due to the long flux buildup time from noise within the cavity. As can be seen in the corresponding right-hand oscillograph, the delay was significantly reduced, by approximately 150 ns, when the XeF(C→A) laser was injected. This reduction in turn-on time is consistent with a model of intracavity flux buildup which we have developed, and with measurements of the small-signal net gain and of the intracavity flux needed to extract energy efficiently from the excited medium. The predictions of this model are shown in Fig. 23 for various flux levels incident upon the partially reflecting mirror of the XeF(C→A) laser cavity. At first the turn-on time decreases with increasing reflectivity due to a reduction in cavity losses and more rapid flux buildup. However, at high reflectivity the turn-on time increases as less flux is transmitted through the mirror into the cavity. At a reflectivity of 82% and an incident flux level of  $5 \times 10^4 \text{ W/cm}^2$ , a turn-on time of approximately 100 ns is predicted, consistent with the observations.

Subsequent to laser turn-on, the XeF(C→A) laser intensity, with injection, as recorded with the broadband filter and photodiode in the diagnostic arm, was almost exactly twice the intensity without injection. This is more clearly shown by the traces in Fig. 24 which represent digitized and replotted versions of the XeF(C→A) laser signals in Fig. 22. To simplify the comparison, the free-running signal was doubled before it was replotted. The 2-to-1 ratio is proof that the XeF(C→A) laser polarization and, therefore, the bandwidth were well controlled by the injected signal. Without injection, the XeF(C→A) laser output was unpolarized. Therefore, only one-half of the laser radiation was routed to the diagnostic arm. The other one-half was transmitted through the Glan-air polarizer, back toward the injection source. However, with injection the XeF(C→A) laser output became circularly polarized, and all of the output was directed into the diagnostic arm. The nearly perfect polarization control without a drop in laser output or efficiency, implies nearly perfect bandwidth control, without a drop in efficiency. Said differently, the 2-to-1 ratio in laser signal amplitudes with and without injection is proof that energy can be extracted efficiently from an XeF(C→A) medium in a narrow spectral band.



N8773

Figure 23. Predicted laser turn-on time as a function of output coupler reflectivity for varying flux incident upon the output coupler.

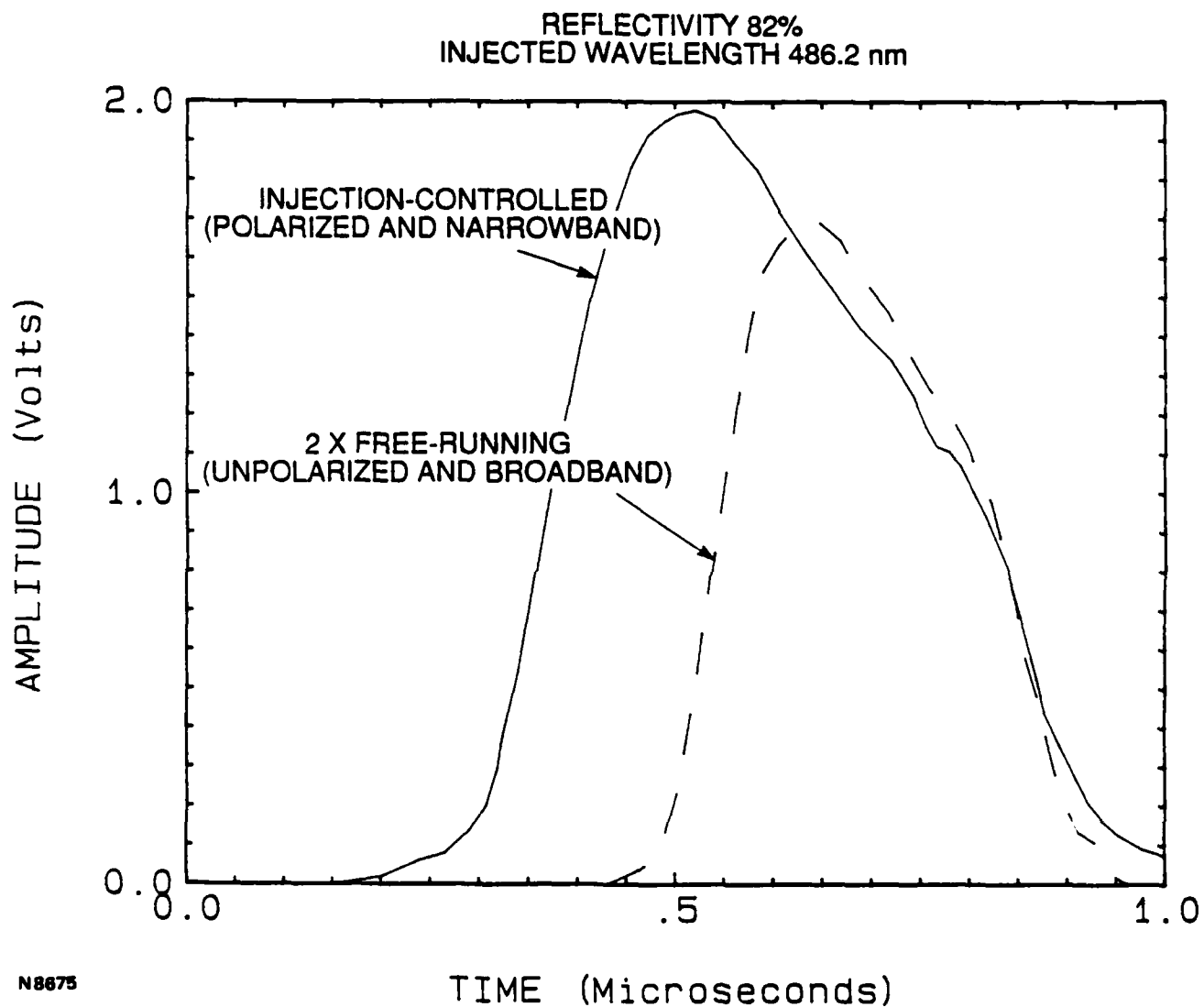


Figure 24. Laser signal amplitude as a function of time for injection-controlled and free-running oscillators. Free-running signal was doubled before plotting.

### 7.3 SPECTRAL CHARACTERISTICS AND WAVELENGTH TUNABILITY

Figure 25 shows measurements of the XeF(C $\rightarrow$ A) laser spectrum at various injected wavelengths, together with the free-running spectrum at 1000 times the sensitivity. The spectra in Fig. 25 were obtained at the higher instrumental resolution of 0.13 nm, obtained with the 2400 line/mm grating. In spite of this, the laser linewidth measured with injection was still instrument-resolution-limited and, hence, represents an upper limit to the actual laser linewidth.

Two of the injection experiments were performed at peaks in the free-running laser spectrum and gave comparable laser outputs. The third experiment was performed in a valley where the free-running laser barely emitted. Nevertheless, a significant amount of energy was extracted even at this wavelength when radiation was injected into the cavity from an external source. The continuously tunable nature of the XeF(C $\rightarrow$ A) laser was thereby demonstrated.

The temporal characteristics of the XeF(C $\rightarrow$ A) laser output at the three injected wavelengths are displayed in Fig. 26. The laser turned on at approximately the same time in the three cases, showing that the net gain during the first 100 ns of the e-beam pulse was similar at these wavelengths. (The same amount of power was injected into the cavity in the three cases.) However, the fact that the laser intensity did not rise as high when the injection source was tuned to a valley in the free-running spectrum suggested a more rapid buildup of absorption at this wavelength during the pulse.

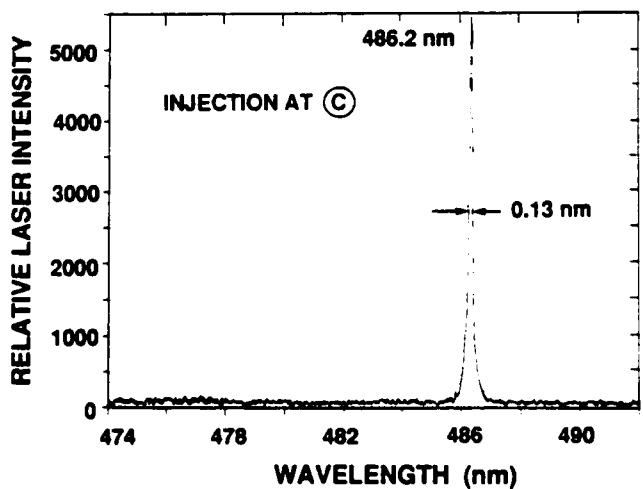
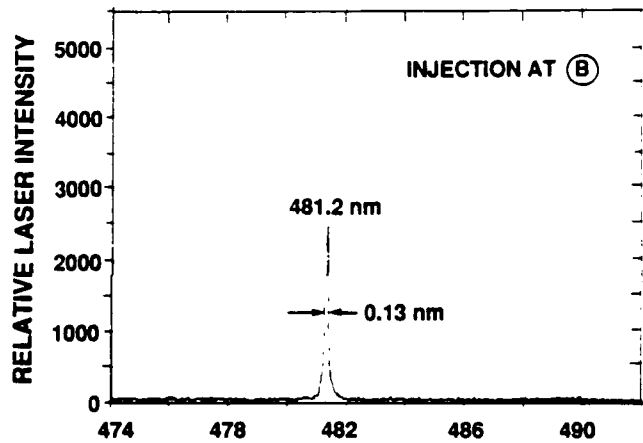
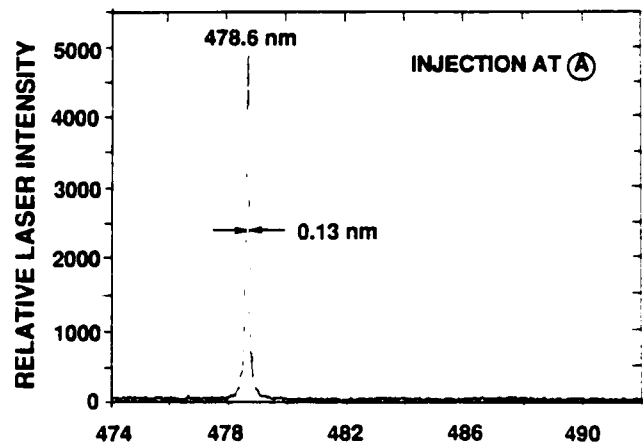
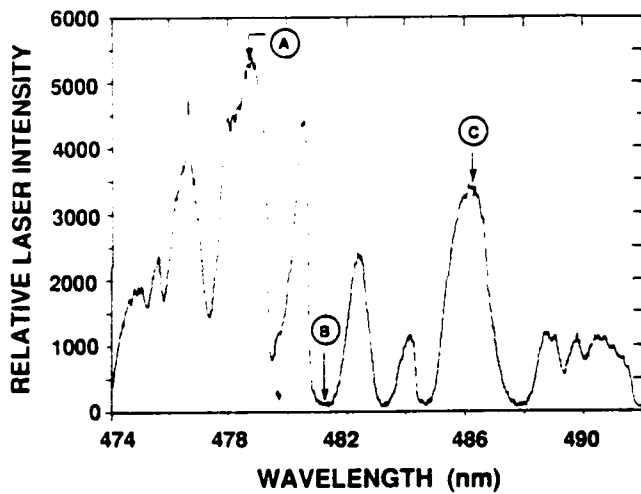
Additional evidence that the XeF(C $\rightarrow$ A) laser is continuously tunable, in spite of the deeply modulated free-running spectrum, comes from the fact that the small-signal net gain which was measured at 488.0 nm, a valley in the free-running spectrum, was only slightly less than that at 476.5 nm, a peak in the free-running spectrum. (See Figs. 19 and 20.) As a result of gain competition in this homogeneously broadened system, small differences in gain show up as much larger modulations in the free-running spectrum.

### 7.4 SUMMARY OF INJECTION-CONTROLLED OSCILLATOR RESULTS

Table 5 summarizes the results that have been achieved with injection. The corresponding numbers without injection were previously presented in Table 4. The intrinsic (energy) efficiency and specific output energy have been increased to 1.8% and 3 J/l, respectively, by means of injection. The laser pulse duration has been extended to 500 ns, and the bandwidth has been reduced to less than 1.3 Å.

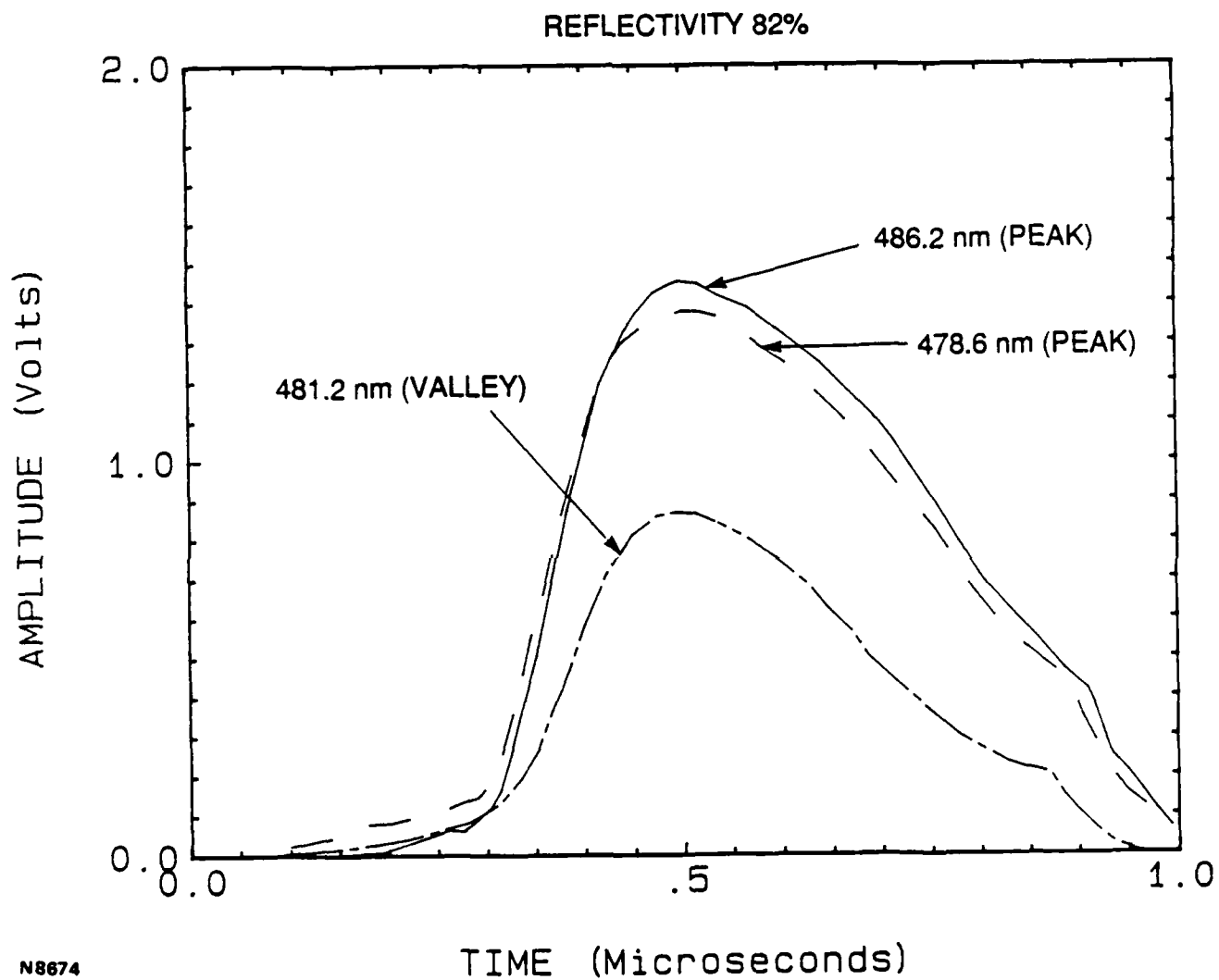
# INJECTION-CONTROLLED SPECTRA

## FREE-RUNNING SPECTRUM (X1000)



N8865

Figure 25. Comparison of free-running oscillator laser spectrum (left side) with injection-controlled oscillator spectra at varying injected wavelength (right side). Instrumental resolution was 0.13 nm. Note the significant reduction in laser bandwidth with injection.



N8674

Figure 26. Temporal pulse shape of injection-controlled laser output at varying injected wavelength.

TABLE 5. SUMMARY OF RESULTS WITH INJECTION

Intrinsic efficiency	1.8%
Specific output energy	3.0 J/liter
Laser pulse duration	500 ns
Laser bandwidth	< 1.3 Å

## 8.0 XeF(B $\rightarrow$ X) LASER PUMP FOR DYE LASER INJECTION SOURCE

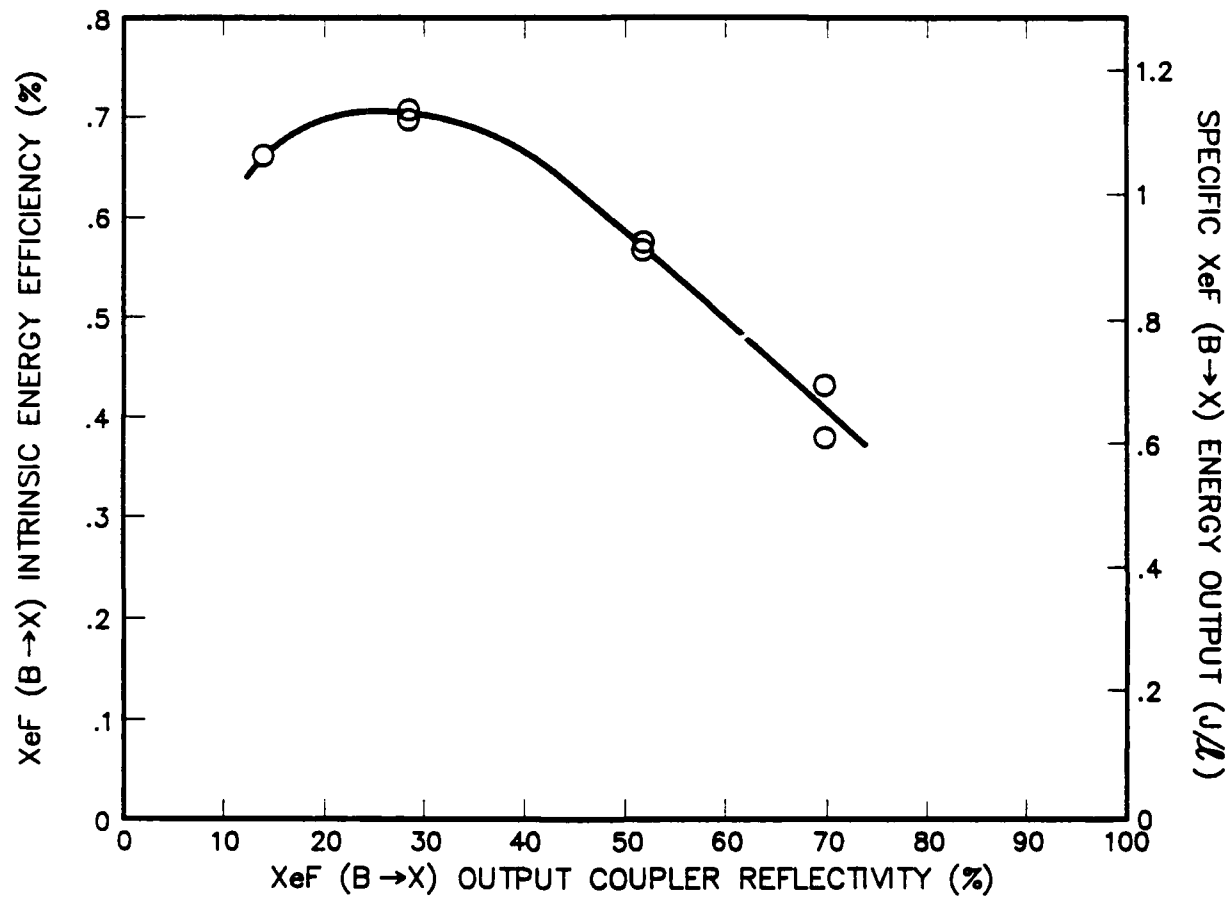
The attainment of maximum energy output from an XeF(C $\rightarrow$ A) laser, with a specified bandwidth and wavelength, requires that the laser cavity be injected with radiation from an external source as the gain begins to rise at the start of the e-beam pulse. Injection allows intracavity flux buildup to start from a level well above noise. This reduces the time required for the flux to reach saturation levels.

A dye laser, pumped by one or more flashlamps, can be used as the injection source. We used such a system during the injection control experiments which are described in Sec. 7.0. An alternative approach would be to pump the dye medium with XeF(B $\rightarrow$ X) laser radiation derived from a portion of the e-beam excited medium. This would eliminate the need for a separate laser with its own power supply, and the requisite synchronization would be achieved automatically.

Because the laser gas mixture had been optimized for maximum XeF(C $\rightarrow$ A) laser output, it was necessary to show that the same gas mixture would support efficient XeF(B $\rightarrow$ X) lasing. Furthermore, for this scheme to work, XeF(B $\rightarrow$ X) laser oscillations would have to be established early in the e-beam excitation pulse so that the XeF(C $\rightarrow$ A) cavity could be injected early in time. Experiments were performed to show that this was the case.

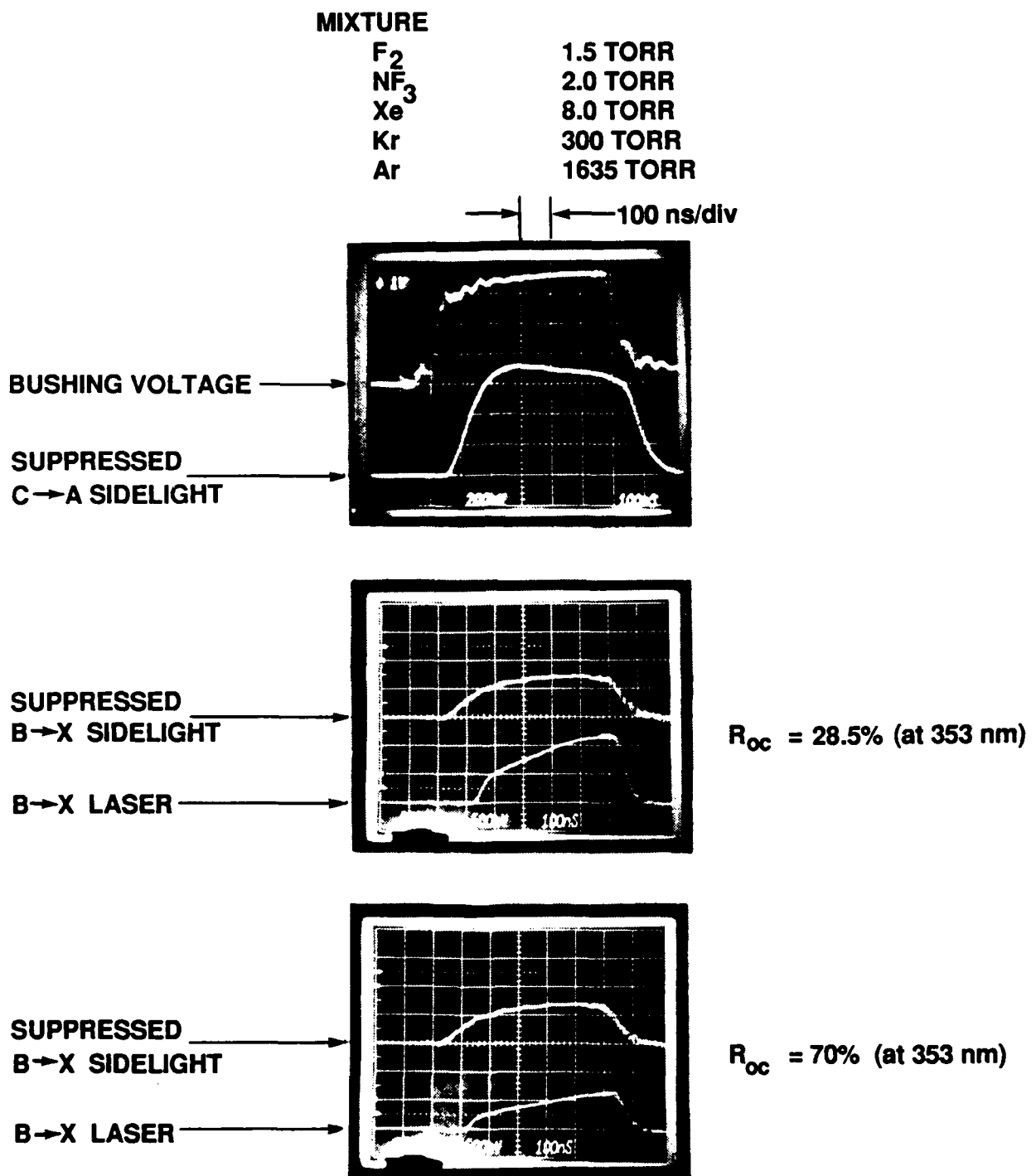
The experimental setup shown in Fig. 2 was utilized. However, the XeF(C $\rightarrow$ A) cavity mirrors were replaced with mirrors which reflected at XeF(B $\rightarrow$ X) laser wavelengths. The filter which was mounted in front of the calorimeter was removed so that XeF(B $\rightarrow$ X) laser radiation could be detected. The reflectivity of the output coupler was varied to establish the optimum value. The results are displayed in Figs. 27 and 28.

Reasonably efficient XeF(B $\rightarrow$ X) lasing was observed, and laser oscillations commenced shortly after the start of e-beam pumping. Specific output energies as high as 1.1 J/l were attained, and the XeF(B $\rightarrow$ X) laser turn-on time was minimized by selecting a high mirror reflectivity. The XeF(B $\rightarrow$ X) laser intensity increased with time during the e-beam pulse, possibly reflecting an increase in the population of the B state as the laser gas was heated by the e-beam. The feasibility of using a portion of the e-beam excited medium to generate pump radiation for a tuned dye laser injection source was thereby demonstrated.



M9327-1

Figure 27. Optimization of XeF(B→X) lasing with XeF(C→A) laser gas mixture.



N6942-1

Figure 28. Temporal characteristics for XeF(C→A) laser gas mixture and XeF(B→X) mirrors.

## 9.0 COMPARISON WITH XeF(C→A) LASER PERFORMANCE AT HIGH E-BEAM PUMP RATE

Table 6 compares the XeF(C→A) results achieved in our laboratory under scalable, low e-beam pump rate conditions, with the results obtained at high e-beam pump rate by Rice University and UTRC (occasionally in collaboration with Max-Planck Institut fur Biophysikalische Chemie).<sup>11</sup> The highest output energies (both total and per unit volume) and the highest intrinsic efficiency have been achieved at low e-beam pump rate. At high e-beam pump rate, efficient and continuous tuning from 470 to 500 nm has been demonstrated, with a specific output energy of  $\sim 1$  J/l and an intrinsic efficiency of  $\sim 1\%$  shown throughout this range.<sup>8</sup> Amplification of an injected signal has been observed over an even wider range (435 to 535 nm), and a linewidth of 0.01 Å has been achieved.<sup>3</sup> The gain coefficient is naturally lower at the lower pump rate, but the lower gain can easily be offset by an extension of the length of the gain medium.

TABLE 6. DEMONSTRATED XeF(C→A) LASER PERFORMANCE AT LOW AND HIGH E-BEAM PUMP RATES

	Low pump rate, long pulse excitation (0.3 MW/cm <sup>3</sup> , 600 ns)	High pump rate, short pulse excitation (12 MW/cm <sup>3</sup> , 10 ns)
	<u>(ARL)</u>	<u>(Rice/UTRC)</u>
Output energy (J)	4.0	0.7
Specific output energy (J/l)	3.0	1.5
Intrinsic efficiency (%)	1.8	1.2
Laser pulse duration (ns)	500	10
Bandwidth (Å)	< 1.3 <sup>a</sup>	0.01
Tuning range (nm)	479-487 <sup>a</sup>	470-500
Peak net gain (%/cm)	0.4	3.0

- a. The bandwidth and tuning range which were demonstrated at low e-beam pump rate were limited only by the capabilities of the spectrometer and the dye laser characteristics. Significantly narrower bandwidths and wider tuning ranges should be attainable.

## 10.0 CONCLUSIONS

Efficient XeF(C $\rightarrow$ A) lasing has been demonstrated under e-beam pumping conditions which are scalable to large devices. A five-component laser gas mixture at a pressure of 2.6 ATM was pumped at a rate of 290 kW/cm<sup>3</sup> with a 600-ns e-beam pulse. The laser gas mixture and output coupler reflectivity were carefully optimized under free-running conditions, and the laser cavity was then injected with radiation from a flashlamp-pumped dye laser to accelerate laser turn-on.

An intrinsic efficiency of 1.8% and a specific output energy of 3 J/l have been achieved, and a total energy of 4 J has been extracted from the excited medium. These values represent a significant improvement in XeF(C $\rightarrow$ A) laser performance over that achieved by Rice University and UTRC at high excitation rate. The laser bandwidth has been reduced by more than two orders of magnitude to less than 1.3 Å, the resolution of the spectrometer, and continuous tuning from 478.6 to 486.8 nm has been shown. Significantly narrower linewidths and a wider tuning range should be possible.

## REFERENCES

1. G.J. Hirst, C.B. Dane, W.L. Wilson, R. Sauerbrey, F.K. Tittel and W.L. Nighan, "Scaling of an Injection-Controlled XeF(C $\rightarrow$ A) Laser Pumped by a Repetitively Pulsed, High Current Density Electron Beam," Appl. Phys. Lett., vol. 54, no. 19, pp. 1851-1853, May 1989.
2. A. Mandl and L.N. Litzenberger, "Efficient, Long-Pulse XeF(C $\rightarrow$ A) Laser at Moderate Electron Beam Pump Rate," Appl. Phys. Lett., vol. 53, no. 18, pp. 1690-1692, Oct. 1988.
3. F.K. Tittel, G. Marowsky, W.L. Nighan, Y. Zhu, R.A. Sauerbrey and W.L. Wilson, Jr., "Injection-Controlled Tuning of an Electron-Beam Excited XeF(C $\rightarrow$ A) Laser," IEEE J. Quantum Electron., vol. QE-22, no. 11, pp. 2168-2173, Nov. 1986.
4. W.L. Nighan, R.A. Sauerbrey, Y. Zhu, F.K. Tittel and W.L. Wilson, Jr., "Kinetically Tailored Properties of Electron-Beam Excited XeF(C $\rightarrow$ A) and XeF(B $\rightarrow$ X) Laser Media Using an Ar-Kr Buffer Mixture," IEEE J. Quantum Electron., vol. QE-23, no. 2, pp. 253-261, Feb. 1987.
5. A. Mandl and E. Salesky, "Electron Beam Deposition Studies of the Rare Gases," J. Appl. Phys., vol. 60, no. 5, pp. 1565-1568, Sept. 1986.
6. W.L. Nighan, F.K. Tittel, W.L. Wilson, Jr., N. Nishida, Y. Zhu and R. Sauerbrey, "Synthesis of Rare Gas-Halide Mixtures Resulting in Efficient XeF(C $\rightarrow$ A) Laser Oscillation," Appl. Phys. Lett., vol. 45, no. 9, pp. 947-949, Nov. 1984.
7. W.L. Nighan, Y. Nachshon, F.K. Tittel and W.L. Wilson, Jr., "Optimization of Electrically Excited XeF(C $\rightarrow$ A) Laser Performance," Appl. Phys. Lett., vol. 42, no. 12, pp. 1006-1008, June 1983.
8. N. Hamada, R. Sauerbrey, W.L. Wilson, Jr., F.K. Tittel and W.L. Nighan, "Performance Characteristics of an Injection-Controlled Electron-Beam Pumped XeF(C $\rightarrow$ A) Laser System," IEEE J. Quantum Electron., vol. 24, no. 8, pp. 1571-1578, Aug. 1988.
9. Y. Nachshon, F.K. Tittel and W.L. Wilson, Jr., "Efficient XeF(C $\rightarrow$ A) Laser Oscillation Using Electron-Beam Excitation," J. Appl. Phys., vol. 56, no. 1, pp. 36-48, July 1984.
10. H.C. Brashears, Jr. and D.W. Setser, "Transfer and Quenching Rate Constants for XeF(B) and XeF(C) State in Low Vibrational Levels," J. Chem. Phys., vol. 76, no. 10, pp. 4932-4946, May 1982.
11. Some of the intrinsic efficiency and specific output energy values reported by the Rice University/UTRC group prior to August 1988 were later found to be in error. The revised values have been published in Refs. 1 and 8.